



# 1        **Evolution of a long-lived continental arc: a geochemical approach**

## 2                                **(Arequipa Batholith, Southern Peru)**

3  
4        **Sophie Demouy<sup>1</sup>, Mathieu Benoit<sup>2</sup>, Michel de Saint-Blanquat<sup>1</sup>, Jérôme Ganne**  
5        **<sup>1</sup>**

6  
7        <sup>1</sup> -, GET, OMP, Université Paul-Sabatier - CNRS - IRD, 14 avenue Edouard-Belin 31400  
8        Toulouse, France.

9        \*corresponding author: Mathieu.Benoit@get.omp.eu

10

11

## 12        **ABSTRACT**

13        Batholith emplacements within a continental margin may bear witness of a magmatic input  
14        lasting for several million years. Consequently, the geochemical signatures of such sections  
15        are complex, and their understanding in terms of petrological processes, is crucial. The  
16        Arequipa section of the Coastal Batholith of Southern Peru was discontinuously constructed  
17        during several periods of magmatic activity, from the Jurassic to the Paleocene (200-175 Ma,  
18        and 90-60 Ma). Thermobarometric data on amphiboles indicates two main levels of  
19        emplacement at the batholith scale, the deepest between 5 and 7 km in depth and the second  
20        around 3.5 km. The present day outcropping of these different units at the same elevation  
21        argue for a large vertical movement along the Lluçlla Fault System between 76 and 68 Ma.  
22        Both major/trace element contents and Nd-Sr isotopes show a large variability that is not  
23        random. The data dispersion is consistent with a two-staged evolutionary model of the  
24        magmatic arc, inspired by the MASH model: (i) an early stage dominated by hybridization  
25        and fractional crystallization processes, (ii) a late stage in which magmas were homogenized  
26        and mainly evolved by fractional crystallization. The change from one stage to another is  
27        controlled by the thermal state of the crustal arc section, especially the Deep Crustal Hot Zone.



28 Keywords: batholith, magmatic arc, Andes, granites, geochemistry, flair-up, MASH model

## 29 1. INTRODUCTION

30 Along active margins, subduction-related processes lead to the injection of voluminous calc-  
31 alkaline magmatic bodies into the continental crust. In general, only a small volumetric  
32 proportion of these magmas reach the surface as lavas (White et al., 2006). At intermediate  
33 and upper crustal levels, elongated plutonic bodies parallel to the trench are emplaced in  
34 composite batholiths. Their construction is spatially and temporally discontinuous, showing  
35 an alternation of high-flux episodes (HFE's) with magmatic lulls (Cruden and Mc Caffrey,  
36 2001; Ducea, 2001; Haschke et al., 2002; Ducea and Barton, 2007; DeCelles et al., 2009;  
37 Bartley et al., 2008; Miller et al., 2011; Saint-Blanquat et al., 2011). HFE's are generally  
38 responsible for the generation of up to 75-80% of the arc volume within relatively short  
39 periods of 10-15 Ma. In the subduction setting, HFE events occurrence is linked to the  
40 development of a dense root and lower crust melting processes (DeCelles et al. 2009).  
41 Batholiths therefore provide an integrated picture of the evolution of long-lived subducting  
42 margin.

43 Petrological and geochemical studies on continental arc magmas reveal the protracted arc  
44 evolution reflected by the broad range in geochemical signatures within one composite  
45 batholith (Pankhurst et al. 1986; Wilson, M., 1989). Petrological processes related to the  
46 generation of intermediate and silicic arc magmas are 1) magma differentiation by fractional  
47 crystallization (Hamilton, 1983; Sisson and Layne, 1993; Müntener et al., 2001; Grove et al.,  
48 2002, 2003) and 2) contribution from the pre-existing continental crust. The contribution of at  
49 least one crustal component can occur following different processes; (i) through generation of  
50 crustal melts by partial melting of pre-existing ancient crust (Atherton and Petford, 1993;  
51 Tepper et al., 1993; Rapp, 1995) and/or younger mafic cumulates (Dungan and Davidson,  
52 2004) around the mantle-crust transition, and successive mixing with juvenile primary  
53 magmas (ii) by crustal assimilation at various crust's levels, i.e. AFC (DePaolo 1981; Powell  
54 1984) or MASH (Hildreth and Moorbath 1988). Both processes are not mutually exclusive.  
55 Nevertheless, some authors are discussing the efficiency of the AFC process at middle-to



56 shallow crustal levels, based on energetic considerations and geochemical modeling (Spera  
57 and Bohrsen, 2001; Glazner, 2007; Clemens et al., 2009, 2010). A comprehensive model that  
58 integrates these different insights is the deep hot zone model proposed by Annen et al.  
59 (2006b). It provides a thermo-mechanical study that explains the generation of magmas  
60 derived by fractionation of high-pressure assemblages from both hydrous mantle-derived  
61 magmas and crustal liquids produced by partial melting.

62 The Andes is one of the two worldwide major orogens with Himalaya-Tibet, under which the  
63 continental crust currently reaches its maximal thickness. Several seismic studies estimated  
64 the crust to be 70 km-thick below the Central Andean Orocline (CAO, 13°S-28°S) and more  
65 precisely beneath the Western Cordillera, where the volcanic arc is located (Beck et al., 1996;  
66 James, 1971). The crustal thickening is hard to unravel over geological times, nevertheless it  
67 appears that the Andean crust underwent significant thinning prior to 90 Ma (Sempere et al.,  
68 2002), and slowly started its thickening from 90 Ma, before it significantly increased by 30  
69 Ma (Mamani et al., 2010; Ganne et al., 2017).

70 In this paper, we intend to determine the evolution of a section of the Coastal Batholith of  
71 Peru, located in the area of Arequipa (16.5°S) through the Western Cordillera. This section is  
72 part of the more than 1600 km-long linear plutonic belt extending along the western margin of  
73 Peru (Pankhurst et al., 1986). The southern area of Peru is remarkable as: (i) No allochthonous  
74 terrane was accreted since the initiation of the subduction (570 Ma; Cawood 2005). (ii) The  
75 plutonic rocks are partly hosted by a thick Precambrian basement (Shackleton et al., 1979). It  
76 is also an area allowing the study of a long-lived arc history, and the interaction of arc  
77 magmas with an old basement. Moreover, the batholith of Arequipa represents a strong  
78 economic interest as it hosts an open-pit of copper and molybdenum mining complex (Cerro  
79 Verde Mine).

80 To document the geochemical evolution of this magmatic arc, we analysed major and traces  
81 elements (100 samples) and Sr and Nd isotopes (92 samples) were analyzed. We combined  
82 these data with ages obtained on the same sample set by in-situ U-Pb zircon method (Demouy  
83 et al., 2012). In the present study, we propose that the combination of both geochronological



84 data (U-Pb in-situ on zircon) and extensive geochemical studies (bulk rock major and trace  
85 elements and isotopic compositions) is a powerful approach to unravel the magmatic history  
86 of the arc system and to understand the contribution of the juvenile and/or crustal reservoirs in  
87 magmatic arc rocks.

88

## 89 2. GEOLOGICAL SETTING

90 The subduction along the Western coast of the South American plate is active since the  
91 beginning of the Paleozoic (570 Ma; Cawood 2005). Subduction-related magmatism led to  
92 the emplacement of granitic intrusions during the Ordovician (468-440 Ma; Loewy et al.  
93 2004), the Carboniferous to Late Triassic period (325-215 Ma around Cuzco in the present  
94 Eastern Cordillera; Mišković et al. 2009) and during the Meso-Cenozoic. This study concerns  
95 the Liassic to Paleocene period in the Arequipa area.

96 The Costal Batholith of Peru is made up of more than 1000 plutons, extending over a 1600  
97 km-long and 60 km-wide array, 150-200 km away from the present-day trench (Pankhurst et  
98 al., 1986). Close to the city of Arequipa, the plutonic rocks form the 'La Caldera' complex  
99 (Stewart, 1968). They crop out from the Northwest towards the Southeast over nearly 1200  
100 km<sup>2</sup>, in which is located our studied area (80x60 km) (Figure 1). The La Caldera complex is  
101 made up of five principal plutonic units, and structured by three main faults (Le Bel 1985;  
102 Mukasa 1986a; Demouy, 2012; Demouy et al. 2012) (Figure 1). The Lluclla Fault System  
103 (LFS) is the largest accident, which divides the northwestern area of the batholith into  
104 northeastern and southwestern parts. The northeastern part is made of two plutonic units,  
105 intrusive into the Precambrian basement, the Gabbros & Diorites unit (GDU) and the Tiabaya  
106 unit (TU). Field relationship suggests a minimal thickness of 1 km for these units. The  
107 southwestern part corresponds to the Linga unit (LU), made up of an amalgam of several  
108 laccolith-shaped intrusions emplaced concordantly within the sedimentary Jurassic cover, and  
109 were tilted about 35° toward the SW after emplacement as indicated both by the bedding of  
110 the sedimentary country rocks and by the geometry of the contacts. This geometry indicates  
111 that the minimum thickness of this unit is around 8 km. Towards the southeast the





112 voluminous Yarabamba unit (YU) crops out both in the northeastern part and the  
113 southwestern part, postdating the Lluella Fault System activity. At the southeastern extremity  
114 of the batholith section, the Chapi-Churajón unit (CCU) intrudes the basis of the sedimentary  
115 Jurassic cover. The different plutonic intrusions appear to be tabular-shaped, and each unit  
116 corresponds to an amalgamation of several intrusions as a result of a discontinuous magmatic  
117 activity that is a common feature in batholith sections (Saint Blanquat et al., 2011; Leuthold et  
118 al., 2012;).

119 Previous U-Pb geochronological studies conducted on zircon grains, either by ID-TIMS  
120 (Mukasa, 1986a) or in-situ LA-ICPMS (Demouy et al., 2012) indicates two main periods of  
121 activity of the magmatic arc in Arequipa. The first period occurred during the Jurassic,  
122 leading to the emplacement of the Gabbros & Diorites unit (200.0-175.8 Ma), of some  
123 intrusions in the southern part of the studied area (188.4 Ma) and of the Chapi-Churajón  
124 diorite (160.5 Ma). The second main period occurred during the Cretaceous-Paleocene (89.8  
125 to 61.6 Ma), with the emplacement of the Tiabaya, the Linga, and the Yarabamba units. The  
126 emplacements of the Linga and Yarambamba units correspond to the latest period of activity  
127 of the arc (70-60 Ma) that leads to the construction of the largest volumes of the batholith (up  
128 to 75%). It was interpreted as a flare-up event at the batholith scale and a major contribution  
129 to the continental crust construction in this area (Demouy, 2012; Demouy et al., 2012).

130  
131 The plutonic units intrude both the basement and a volcano-sedimentary cover. The basement  
132 is one of the several Proterozoic blocks cropping out in southern Peru and collectively named  
133 “the Arequipa Massif”. Those rocks underwent complex, polycyclic magmatic and  
134 metamorphic history from the Early Proterozoic to the Early Paleozoic. First, a large orogenic  
135 cycle occurred between 2.1-1.8 Ga and then a second main one (Grenvillian event) between  
136 1.2 and 0.97 Ga (Loewy et al., 2004; Casquet et al., 2010). In southern Peru, the Grenvillian  
137 event is described in the Camaná-Mollendo block between 1040 and 940 Ma (Martignole and  
138 Martelat, 2003; Casquet et al., 2010). The basement is overlain by a thick stratigraphic  
139 succession of Late Paleozoic to Neogene age, made of both volcanoclastic arc products and  
140 marine to continental sediments. The Paleozoic-Mesozoic part of this succession in the



141 Arequipa area is about 5 km-thick and is locally intruded by Jurassic to Paleogene intrusive  
142 rocks (Cruz, 2002; Sempere et al., 2002; Boekhout et al., 2013).

143

### 144 3. SAMPLING AND ANALYTICAL PROTOCOL

#### 145 3.1 Sampling

146 The sampling was conducted following two rules: (i) take a large number of samples in each  
147 plutonic unit, (ii) avoid bias by sampling regularly each plutonic unit (maximum ~2km  
148 between each location) even if there is no field evidence of change in the mineralogy. We  
149 consider that this sampling strategy is well adapted to study both intra-and inter-plutonic  
150 petrological and geochemical variability. Sampling was mainly conducted along three main  
151 cross-sections, perpendicular to the NW-SE trend of the batholith. Intermediate and peripheral  
152 locations around the cross-sections were also sampled towards the NW, the SE and the  
153 southern parts of the study area (Figure 1). The location and main characteristics of each of  
154 the 100 samples selected for the geochemical study are listed in the Supplement A.

155

#### 156 3.2 Analytical protocol

157 Quantitative analyses on mineral phases were performed at Université de Toulouse, GET  
158 (France) using a CAMECA SX50 microprobe with SAMx automation. The operating  
159 conditions were: accelerating voltage 15 kV, beam current 10nA or 20 nA (depending on the  
160 resistance of the mineral to beam damage) and analyzed surface 2x2  $\mu\text{m}^2$ . Natural and  
161 synthetic minerals have been used as standards. Major and trace element abundances were  
162 acquired in SARM, Nancy (France) and ALS Mineral, Seville (Spain) by inductively coupled  
163 plasma atomic emission spectrometry (ICP-AES) and inductively coupled plasma mass  
164 spectrometry (ICP-MS) after LiBO<sub>2</sub> fluxing. For isotopic measurement, we proceed to acid  
165 digestion (HNO<sub>3</sub>-HF-H<sub>2</sub>O<sub>2</sub>) before evaporation and chemical separations. We used Eichrom  
166 Sr-SPEC and TRU-SPEC resins for Sr and REE elutions, respectively, and LN-SPEC resin



167 for Nd elution. Sr, Nd isotopic ratios were measured using a Finnigan MAT-261 mass  
168 spectrometer. Repeated analyses of the NBS 987 standard yielded an average value of  $^{87}\text{Sr}/^{86}\text{Sr}$   
169  $= 0.710238 \pm 8$  ( $2\sigma$ ,  $n=7$ ) with a standard deviation of  $1.09 \times 10^{-5}$ . Repeated analyses of the La  
170 Jolla standard yielded an average value of  $^{143}\text{Nd}/^{144}\text{Nd} = 0.511846 \pm 6$  ( $2\sigma$ ,  $n=9$ ) with a standard  
171 deviation of  $6.01 \times 10^{-6}$ . The blank for Sr and Nd are negligible with quantities  $<200$  pg for Sr  
172 and  $<50$  pg for Nd.

173

#### 174 4. PETROGRAPHY AND MINERAL CHARACTERISTICS

175 The plutonic units are defined through structural and petrological arguments. Each unit is  
176 made up of one or several plutons. In order to describe the different units we use the  
177 terminology defined by (Le Bel, 1985), who published the most detailed petrological study in  
178 this area. At the batholith's section scale, there are no large variations of the mineralogy for a  
179 given lithology from one unit to the other. Hence, to complete the general petrological  
180 observations by unit listed above, the characteristics of the main mineral phases are reported  
181 in Table 1.

182 • The Gabbros & Diorites unit is made of gabbros and diorites sensus lato (diorite and quartz-  
183 diorites, (Cox et al., 1979). The entire unit is located in the NE part of the batholith, and  
184 intrudes the Precambrian basement. It is locally affected by ductile and brittle deformations  
185 and is widely cut by thick (up to 10 m-wide), EW-trending, steeply dipping basaltic and  
186 granitic dykes. We identify amphibole-bearing and quartz-bearing gabbros. The average  
187 mineralogy for gabbros is  $\text{Plg} + \text{Px} + \text{Amph} + \text{Ox} \pm \text{Qz}$ . One of the gabbroic samples  
188 corresponds to the oldest rock dated in the batholith ( $200.0 \pm 1.2$  Ma, Demouy et al. 2012).  
189 Some of the gabbros display cumulative textures with clinopyroxenes and plagioclases as  
190 cumulate phases (figure 2), and the other phases like amphibole and titanite are inter-cumulate  
191 phases. Diorites sensu stricto dominate the unit displaying a classical mineralogy:  $\text{Plg} \pm \text{Px}$   
192  $+ \text{Amph} + \text{Bt} \pm \text{Kf} + \text{Ox} + \text{Qz}$ . The youngest age obtained in the Gabbros & Diorites unit  
193 corresponds to a quartz-diorite sample, which is the less represented facies ( $175.8 \pm 1.2$  Ma,  
194 Demouy et al. 2012).



- 195 • The Chapi-Churajón diorite is composed of two main intrusions. They both intrude the  
196 Jurassic sedimentary cover and are located at the most southeastern part of the studied area.  
197 The dioritic intrusion is located toward the southeast and the quartz-dioritic towards the  
198 northwest. The mineral assemblages of these two facies are uncommon at the batholith scale,  
199 characterized by the absence of amphibole and the occurrence of porphyritic K-feldspar (0.5-  
200 1.5 cm).
- 201 • The Tiabaya unit is made of two plutons (SE and NW), located in the northeastern part of  
202 the batholith. It mainly intrudes the Liassic component of the batholith (Gabbros & Diorites  
203 unit), and locally the Precambrian basement (Tiabaya-SE only). Each pluton is homogeneous  
204 considering the texture and the mineralogy of the rocks. Tiabaya NW is made of diorite and  
205 Tiabaya SE of quartz-diorite. Mineral assemblages are  $\text{Plg} \pm \text{Px} + \text{Amph} + \text{Bt} + \text{Ox} + \text{Kf} + \text{Sph}$   
206  $+ \text{Zr}$ . Ferro-magnesian minerals are euhedral and can reach several millimeters in the Tiabaya  
207 SE unit. Some amphiboles display clinopyroxene cores in the Tiabaya NW unit.
- 208 • The Linga unit is intrusive within the Jurassic sedimentary strata. It constitutes the  
209 southwestern part of the batholith and is made of several massive gabbrodioritic, dioritic,  
210 quartz-dioritic and granitic tabular bodies. As for the Gabbros & Diorites unit, the gabbros  
211 locally present cumulative characteristics. Diorites and quartz-diorites constitute the largest  
212 outcrops of the unit, and the granites are spatially restricted to the southwestern end of the San  
213 Jose Quebrada (Figure 1).
- 214 • The Yarabamba unit is mainly quartz-dioritic and intrudes the precambrian basement, the  
215 Chapi-Churajón diorite, the Tiabaya SE pluton, the Linga unit and the Jurassic sedimentary  
216 cover. The porphyry copper of the Cerro Verde Mine is associated with the micro-quartz-  
217 diorite facies of the Yarabamba unit, and a large part of the unit remains hidden under  
218 recent deposits. The Yarabamba unit is mainly made of quartz-diorites but we also identified  
219 some gabbro-diorites and granites scattered in the unit. Mineral assemblages for the quartz-  
220 diorite are similar to those of the Linga unit with  $\text{Plg} \pm \text{Amph} + \text{Bt} + \text{Ox} + \text{Kf}$ .



221 All the plutons of the studied area locally contain mafic enclaves and display magmatic  
222 fabrics and textures with rare clear evidences of magmatic foliation. They contain little  
223 evidences of post-emplacement deformation.

224

## 225 5. AMPHIBOLE THERMOBAROMETRY

226 We analyzed the amphibole grains of 16 samples from: basement (n: 1), Linga unit (n: 5),  
227 Tiabaya unit (n: 5) and Yarabamba unit (n: 1). The data are listed in Supplement B and  
228 plotted in Figure 3a and b and in figure 4 for P/T estimates. The range of temperature  
229 calculated is 904 to 662 C°, and the corresponding range of pressure is 3.3 to 0.4 kbar (Figure  
230 4). The pressures correspond to upper crustal emplacement conditions (up to 13 km), and  
231 temperatures are consistent with those indicated in the literature for calc-alkaline magmas  
232 (Ridolfi and Renzulli, 2012). We observe both inter-and intra-plutonic units variations.

233 In Jurassic plutons, amphiboles indicate a 901-692°C crystallization temperatures range for  
234 two different range of pressure: 1.9-1.0 kbar for the cumulative 09SD226 rock and 1.3-0.4  
235 kbar for the 09SD221 and 09SD265 gabbros. The Cretaceous rocks are characterized by three  
236 different pressure ranges: (i) Linga 09SD012 (P: 0.9-0.7 kbar) (ii) Tiabaya 09SD31-33-34-  
237 164 (P: 1.6-1.1 kbar) (iii) Tiabaya 06SD160 mafic enclave (P: 3.5-1.2 kbar). Between theses  
238 three sets, the temperatures does not significantly differ and range from 829 to 662°C. The  
239 Maastrichtian-Paleocene rocks constitute a homogeneous set of data (P: 1.0-0.5 kbar and T:  
240 789-668°C). The highest range of pressures corresponds to the amphiboles of the basement  
241 sample (3.5-2.2 kbar; T: 863-766°C).

242 To sum up, we find three main ranges of pressure (i) a low range (P: 0.4-1.6 kbar)  
243 corresponding to the Gabbro & Diorite, Linga and Yarabamba units (ii) a middle range (P:  
244 1.0-1.9 kbar) corresponding to the Tiabaya NW unit and a cumulative rock from Gabbro &  
245 Diorite unit. (iii) a high range (P : 1.2-4.5 kbar) corresponding to a mafic enclave in Tiabaya  
246 NW unit and the basement sample.

247



## 248 6. WHOLE ROCK GEOCHEMICAL DATA

### 249 6.1 Major elements

250 The major and trace element data is given in Supplement C. TAS diagram shows that the data  
 251 are in good accordance with the petrographic description (Figure 5a). As a whole, samples  
 252 from various periods of activity define trends that partly overlap themselves, fitting the calc-  
 253 alkaline trend (Figure 5b). The six most mafic rocks (Gabbro & Diorite unit) that plot in the  
 254 tholeiitic area are cumulative rocks, this explains their higher Fe content regarding the other  
 255 samples. The A/CNK and A/NK molar ratios of the samples are negatively correlated,  
 256 defining a large trend from the mafic to the felsic rocks (Figure 5c). Most of the sample set  
 257 plot in the metaluminous area, and only the most evolved samples from the Jurassic rock set  
 258 (quartz-diorites) and the Cretaceous granites display peraluminous affinities. Two samples are  
 259 clearly peraluminous with A/CNK molar ratios  $>1.1$ , corresponding to two quartz-diorites  
 260 from the Gabbro & Diorite unit, i.e. the youngest and the most differentiated rocks of this unit  
 261 (09SD10 and 09SD27). The A/CNK ranges are high for the Jurassic (0.66-1.21) and the  
 262 Cretaceous (0.70-1.06) rocks, whereas for the Maastrichtian-Paleocene it is narrower (0.80-  
 263 0.98). To sum up, according to the major elements, the sample set is made of three sample  
 264 groups characteristic of typical of arc-magmatism that do not significantly differ as a function  
 265 of their respective ages. Nevertheless, the youngest sample set (Maastrichtian-Paleocene)  
 266 display less Major Element variations than the oldest sets.

267

### 268 6.2 Trace elements

269 As a whole, the trace elements patterns of our sample set are characteristics from arc-related  
 270 Andean plutonic rocks (Figure 6 a and b).

271 The REE patterns of the entire sample set display common features with a light rare earth  
 272 element (LREE)-enrichment (Figure 6a) and  $(La/Yb)_n$  ratios ranging from 2.4 to 20.2. For  
 273 each age group LREE fractionation increases with the differentiation degree of the rocks in  
 274 similar proportion. For all samples, the  $(La/Sm)_n$  ratio rises from gabbros and gabbro-diorites



275  $[(La/Sm)_n = 1.4-4.4]$  through diorites and quartz-diorites  $[(La/Sm)_n = 1.8-6.4]$  to granitic rocks  
276  $[(La/Sm)_n = 2.7-6.4]$ . The gabbros display lower normalized La and Yb values ( $La_n = 9.8-89.4$ ,  
277  $Yb_n = 2.9-14.9$ ) than the diorites and quartz-diorites ( $La_n = 37.9-189.4$ ,  $Yb_n = 6.3-21.7$ ) and the  
278 granites ( $La_n = 62.6-161.7$ ,  $Yb_n = 8.3-21.5$ ). Surprisingly, the most enriched rocks belong to the  
279 dioritic group, and not the granite one. Two samples from the Gabbro & Diorite unit  
280 (09SD232) and the Lingua unit (09SD17) display strong positive Eu anomalies, with  $Eu/Eu^*$   
281 ratios  $>1.5$ , and are consistent with the cumulate textures mentioned in the petrological study.  
282 Indeed, plagioclase is one major phase in the mineralogy of these cumulative samples.

283 Except for the cumulative rocks, primitive mantle-normalized trace element patterns indicate  
284 similar geochemical characteristics for most of the rock types, and some differences appear in  
285 the relative size of the anomalies (Figure 6b). Most samples show positive anomalies in some  
286 LIL elements as Cs, Rb, U, Pb, Sr and also for Th and K, and relative depletions in HFS  
287 elements as Nb, Ta and also Ti and P. These features correspond to classical signatures of  
288 subduction-related magmas (McCulloch and Gamble, 1991). Nb negative anomaly is more  
289 pronounced in the intermediate and felsic rocks [granites:  $(Nb/La)_n = 0.16-0.54$ ] than in the  
290 mafic rocks [gabbro-diorites :  $(Nb/La)_n = 0.13-0.24$ ], as the negative Ti anomaly.

291

### 292 *6.3 Sr and Nd isotopic data*

293

294 Whole rock Sr and Nd isotopic data are reported in Supplement D along with Rb, Sr, Sm and  
295 Nd concentrations.

296 The  $^{87}Sr/^{86}Sr_m$  range is large with values comprised between 0.70528 and 0.71788, as illustrated  
297 in the Rb-Sr isochron diagram (Figure 7). This figure highlights two different set of samples:  
298 (i) the first set is made of samples characterized by a narrow range of  $^{87}Rb/^{86}Sr_m$  ratio (0.14–  
299 1.18) for a large range of  $^{87}Sr/^{86}Sr_m$  ratio (0.70545–0.71279), with a scattered repartition. This  
300 domain includes all of the Jurassic samples (n: 20), the Cretaceous samples of the Tiabaya  
301 NW unit (n: 7), and several samples of the Yarabamba unit (n: 5). (ii) the second set contains



302 samples characterized by a large range of both  $^{87}\text{Rb}/^{86}\text{Sr}_i$  and  $^{87}\text{Sr}/^{86}\text{Sr}_m$  ratio. The data align  
303 themselves, and these alignments are often interpreted as errorchrons in isochron diagrams.  
304 According to field, geochronological and geochemical data, all samples that fall along the  
305 calculated errorchrons are age-consistent (Figure 7). Therefore, we propose that these  
306 alignments do not correspond to mixing lines. The Cretaceous samples of the Lingua unit  
307 define three errorchrons (respectively estimated at 86, 88 and 89 Ma) that fall along a  
308 calculated Rb-Sr isochron calculated using U-Pb data from the sample 09SD275 ( $87.1 \pm 1.0$   
309 Ma,  $^{87}\text{Sr}/^{86}\text{Sr}_i = 0.70591$ ): (i) the Linga-QLK group (n: 3), (ii) the Linga-SJK2 group (n: 6), (iii)  
310 the Linga-OPK group (n: 9). The Rb-Sr age's estimates are consistent with the U-Pb  
311 cretaceous ages previously obtained in this area ( $89.8 \pm 0.7$  Ma and  $87.7 \pm 1.0$  Ma). The  
312 Maastrichtian-Paleocene samples (Linga-QLP, -SJP and -PAP, n: 23) fall along an 63.7  
313 errorchron, which is consistent with the calculated Rb-Sr isochrones from samples 09SD318A,  
314 09SD312, 09SD308 and 09SD18: respectively dated at  $68.7 \pm 0.5$  and  $65.5 \pm 0.4$  Ma  
315 (Demouy et al., 2012).

316  $^{143}\text{Nd}/^{144}\text{Nd}_m$  ratios range from 0.51208 to 0.51266, and their positioning in the Sm-Nd isochron  
317 diagram (Figure 8) is scattered, with no clear distinction between Jurassic, Cretaceous and  
318 Maastrichtian-Paleocene signatures. Nevertheless, the El Toro and Chapi-Churajón groups  
319 display higher  $^{143}\text{Nd}/^{144}\text{Nd}_m$  ratios (0.51244-0.51266) than the Gabbro & Diorite unit  
320 (0.51224-0.51260). We identify a set of 54 cretaceous and Maastrichtian-Paleocene samples  
321 concentrated within an area defined by  $^{143}\text{Nd}/^{144}\text{Nd}_m$  values between 0.51244 and 0.51259 and  
322  $^{147}\text{Sm}/^{144}\text{Nd}_i$  values between 0.109 and 0.135. 9 samples plot outside of this area, corresponding  
323 to the Linga-QLK group (n: 3), 3 samples from the Yarabamba unit, 2 samples of the Linga-  
324 SJK1 group and 1 sample from the Tiabaya unit.

325 According to these results, we have performed age corrections for the measured samples. Two  
326 scenarios have been investigated: (i) samples that are falling on a single errorchron should  
327 have the same initial isotopic ratio. (ii) samples, which have been dated by U/Pb method  
328 should be corrected from their own ages, and for the other ones we use estimated ages (both  
329 errorchrons or regional ages). We have decided to use option (ii) because option (i) is not





330 applicable to Sm/Nd isotopic system and, for example, some of Maastrichtian-Paleocene  
331 samples that fall on the estimated errochron gave different U/Pb ages. Following this, initial  
332 isotopic ratios ranges are 0.70428 to 0.71095 for  $^{87}\text{Sr}/^{86}\text{Sr}$  and 0.51202 to 0.51253 for  $^{143}\text{Nd}/^{144}\text{Nd}$ ,  
333 ( $\epsilon\text{Nd}$  from -10.4 to +1.71) for the whole dataset. They are reported in figure 9. Except for two  
334 jurassic samples from the El Toro area (related to the Ilo batholith), all samples plot in the  
335 crustal array and their positioning is significantly scattered. At a whole scale, we may observe  
336 a decrease of the scattering with time, pointing toward more juvenile signatures (Figure 9).  
337 This feature will be discussed in detail in the following sections.

338

## 339 7. DISCUSSION

### 340 7.1 Vertical movements during batholith emplacement

341

342 The Andes is one of the two worldwide major orogens with Himalaya-Tibet, under which the  
343 continental crust currently reaches its maximal thickness. Several seismic studies estimated  
344 the crust to be 70 km-thick below the Central Andean Orocline (CAO, 13°S-28°S) and more  
345 precisely beneath the Western Cordillera, where the volcanic arc is located (Beck et al., 1996;  
346 James, 1971). The crustal thickening is hard to unravel over geological times, nevertheless it  
347 appears that the Andean crust underwent significant thinning prior to 90 Ma (Sempere et al.,  
348 2002), and slowly started its thickening from 90 Ma, before it significantly increased by 30  
349 Ma (Mamani et al., 2010).

350 In the Arequipa batholith, field and geochronological data constrain the timing and general  
351 organization of the plutonic units. Nevertheless, details on the functioning of the main  
352 accident affecting the batholith (Llucella Fault System in particular) still remain a matter of  
353 debate. The movements linked to the faults have caused vertical displacements of the plutonic  
354 units that need to be quantified (Demouy et al., 2012).

355 The plutonic unit that currently crops out at the surface might have crystallized at different  
356 crustal depths, and granitoids barometry can play a critical role in constraining tectonic



357 history (Smith et al., 1998). In the Arequipa batholith, the barometric data suggest two main  
358 levels of plutonic magma emplacement: a shallowest level (P: 0.4-1.6 kbar) for the  
359 Yarabamba, Linga and the Gabbros & Diorites units (apart from cumulate 09SD221), and a  
360 deepest level (P: 1.0-1.9 kbar) for the Tiabaya unit and the cumulative 09SD221 G&D sample.  
361 The amphiboles from the basement display higher crystallization pressures than in the  
362 plutonic units, attesting that the basement was exhumed before the pluton emplacement.

363 We observe both intra- and inter-plutonic unit discrepancies in terms of amphibole  
364 crystallization pressures. For the intra-plutonic unit variations: (i) within the Gabbros &  
365 Diorites unit, the gabbro 09SD221 and the related cumulative gabbro 09SD226 record  
366 different amphibole crystallization pressures. Results support the hypothesis of an early  
367 crystallization of some of the cumulative phases (1.6 kbar in average), rather than a complete  
368 magma differentiation at the batholith emplacement level (0.8 kbar in average); (ii) within the  
369 Tiabaya unit, highest amphibole crystallization pressures than in the surrounding dioritic  
370 samples characterize the large mafic enclave 09SD160. The enclave may have been extracted  
371 and dragged towards the surface by the dioritic magmas. The barometric data for the enclave  
372 range between 3.2 and 1.2 kbar supporting the idea of re-or syn-crystallization of amphiboles  
373 during the magma's ascent.

374 For the inter-plutonic unit variations: (i) The Jurassic rocks from G&D unit, apart from the  
375 cumulative one, correspond to the lower pressure range (P: 0.4-1.6 kbar) at the batholith scale.  
376 This unit (200 and 175 Ma, Demouy et al. 2012) crosscuts the basement of the Arequipa  
377 batholith. The emplacement depth of the magmatic unit is poorly constrained by the field  
378 observations. (ii) The Cretaceous rocks crop out both in the actual Northeastern part and the  
379 Southwestern part of the batholith, in the Tiabaya and the Linga units, respectively. The  
380 Cretaceous rocks emplaced at shallow (in the Southwestern part) or deeper crustal level (in  
381 Northeastern part), depending on their location.

382 According to the barometric data, the Tiabaya unit and the crosscutting Gabbros & Diorites  
383 unit did not emplace at the same level, and Cretaceous rocks emplaced at different depths on  
384 each side of the Lluçla faults System (Figure 10). Considerable crustal thinning occurred in



385 the Early Jurassic and culminated in the Middle Jurassic, leading to considerable subsidence  
386 in the Arequipa basin in southern Peru. This is shown by the accumulation of a 4500-6000-m-  
387 thick pile of Jurassic sediments (Yura Group, Sempere et al. 2002), covered by 500-1000-m-  
388 thick Cretaceous marine deposits. Hence, the Gabbros & Diorites unit that emplaced between  
389 200 and 175 Ma at shallow level (P: 0.4-1.1 kbar) was buried during the Jurassic. At 90Ma,  
390 the thick sedimentary pile accumulated made possible different levels of emplacement for the  
391 Cretaceous arc magmas. In the Southwestern part, the magmas of the Linga unit emplaced  
392 between the Labra and Cachios formations, i.e. at approximately 3.5 km in depth. The  
393 amphiboles record pressures between 0.7 and 0.9 kbar. On the NE side of the Lluclla Fault  
394 System, the Tiabaya unit crosscuts the Gabbros & Diorites unit at a deeper level, with  
395 pressures ranging from 1.1 to 1.6 kbar. Following the estimation from the Linga unit, this  
396 indicates an emplacement level between 5-7 km. Starting at 69 Ma, the emplacement of the  
397 plutonic rocks occurred at the same level (Linga unit level), north and south of the Lluclla  
398 Fault System. This observation suggests that the northeast part of the batholith, that is the  
399 footwall of the Lluclla normal fault, was exhumed with a 1.5 to 3.5 km vertical movement in  
400 less than 10 Ma (between 76 and 68 Ma). The growth of the Coastal Batholith could be  
401 responsible of these extensional movements, which has to occur in a convergent geodynamic  
402 context. The emplacement of the Yarabamba unit clearly postdates the activity of the Lluclla  
403 Fault System at 66 Ma.

## 404 *7.2 The geochemical variability of the Arequipa's batholith's magmas*

405

### 406 *7.2.1 Observations and questions*

407 The geochemical signatures recorded by the igneous rocks of the Arequipa's section of the  
408 Coastal Batholith of Southern Peru show a broad diversity, which mimics what has been  
409 already observed in several other batholith sections (e.g. Sierra Nevada and Chilean  
410 batholiths; DePaolo 1981; Herve et al. 2007; Parada et al. 2007; DeCelles et al. 2009). The  
411 Jurassic, Cretaceous and Maastrichtian-Paleocene rocks of the Arequipa batholith section  
412 have the Nd and Sr isotopic compositions expected for subduction related igneous rocks  
413 (Figure 9). The data spread from the mantellic to the crustal quadrant, i.e. from the almost



414 juvenile to strong crustal signatures. Each period of activity of the arc display different  
415 characteristics:

416 • Within the whole dataset, the Jurassic rocks display the largest  $^{87}\text{Sr}/^{86}\text{Sr}$  and  $\epsilon\text{Nd}$  ranges. On  
417 one side, the El Toro and Chapi-Churajón units display the most depleted, mantle-like  
418 signatures ( $\epsilon\text{Nd}$  up to +1.7). On the other side, the Gabbros & Diorites unit displays a large  
419 range of  $^{87}\text{Sr}/^{86}\text{Sr}$ , the highest value (0.71095) corresponding to the mafic oldest sample  
420 (gabbro 09SD221,  $200.0 \pm 1.1$  Ma, Figure 9).

421 • The Maastrichtian to Paleocene rocks display a narrow range of isotopic signatures  
422 ( $^{87}\text{Sr}/^{86}\text{Sr}$  for Linga unit: 0.70516-0.70655), apart from three samples from the Yarabamba  
423 unit that were collected close to the borders of the unit.

424 • The Cretaceous rocks display intermediate isotopic signatures between the Jurassic and the  
425 Maastrichtian to Paleocene rocks. We observe a decrease in the isotopic heterogeneity starting  
426 from the oldest (Linga-SJK1) to the youngest (Tiabaya) samples. The youngest ones from the  
427 Tiabaya unit display the most juvenile signatures.

428 Besides the fact that a clear time gap exists between each plutonic unit emplacement episode,  
429 the isotopic variability tends to diminish with time and restricts itself in a domain located  
430 between the Ilo and the Upper Paleozoic Chilean areas in Figure 9. The simplest hypothesis  
431 would be that a different magmatic process characterizes each period of magmatic activity.  
432 However, there is an apparent paradox: the magmatic activity is discontinuous in the area, but  
433 if we consider all of the plutonic units as a whole; the more mafic, the more – isotopically -  
434 heterogeneous it is. This feature is the exact opposite to what the AFC process predicted  
435 (DePaolo, 1981). Given this paradox, the next section will address the two following  
436 questions:

437 1. Which process can explain the trace element and isotopic diversity encountered within each  
438 plutonic unit?



439 2. Why this heterogeneity becomes less and less pronounced in the youngest and more  
440 evolved samples?

441 Previous studies mentioned the broad geochemical diversity of the rocks from the southern  
442 Coastal Batholith of Peru (Tilton and Barreiro, 1980; Mukasa, 1986b; Boily et al., 1989) and  
443 underline the involvement of the Arequipa continental crust in the genesis of the arc magmas.  
444 However, it is at first glance difficult to vanish any juvenile input at the crust basis. Large  
445 chemical variations in worldwide batholithic rocks are commonly observed, and many  
446 different mechanisms have been considered to explain their acquisition. These mechanisms  
447 involve mixing/hybridization of magmas, and/or differentiation of the parental magmas (see  
448 review in Clemens and Stevens, 2012). They were at first envisioned at various crustal levels,  
449 from the depth closest to the magma source to higher levels in the uppermost magmatic  
450 systems. The most popular model to explain more particularly the isotopic variation in the  
451 batholiths is the AFC model (DePaolo, 1981) that combines the assimilation of the crustal  
452 wall-rock with the differentiation of the rocks. Because assimilation is energy consuming,  
453 these mechanisms might be more efficient at lower levels than at higher levels of the crust  
454 (Spera and Bohrsen, 2001; Glazner, 2007).

#### 455 *7.2.2 Data exploration*

456 Previous work on the Southern Peruvian Coastal Batholith proposed a two-step AFC model  
457 involving first a lower Precambrian crust and then a middle upper Precambrian crust - to  
458 explain the geochemical and isotopic diversity of the different plutonic rocks (Boily et al.,  
459 1989). Our dataset is clearly not consistent with an AFC model, as explained before.  
460 Moreover, regarding isotopes, several samples should have undergone excessive amount of  
461 combined assimilation and fractionation to explain their enriched signatures. This is  
462 inconsistent with their mafic compositions. In order to assess the questions listed before we  
463 have used Rb-Sr plots, in which we have reported the sample signatures (Figure 7). This  
464 approach allows us to draw some global sketches and isolate groups with specific elemental  
465 Rb/Sr ratios and Sr isotopic characteristics. They are listed hereafter:



466 • The Maastrichtian-Paleocene (MP) group includes 23 samples (diorites and quartz-diorites)  
467 issued from the Linga-QLP, -SJP and -PAP samples. Within this group, the samples cluster  
468 around a straight line. According to the U-Pb ages obtained on several samples from the MP-  
469 group (Maastrichtian-Paleocene ages, Demouy et al. 2012), we have superimposed on the  
470 data isochrones calculated from these ages. We observe that the distribution of the MP-group  
471 dataset fits with the domain defined by the calculated isochrones. This suggests that this trend  
472 corresponds to an errorchron and not to a mixing-line. The initial  $^{87}\text{Sr}/^{86}\text{Sr}$  ratio indicated by the  
473 errorchron (or whole rock isochron) is  $0.705364 \pm 0.000081$ .

474 • The Cretaceous (K) group includes the Linga -SJK2 (n: 3) and OPK samples (n: 8). Each  
475 dataset plots on a distinct trend. As for the MP-group, we calculated isochrones from the  
476 Cretaceous U-Pb ages of the Linga unit. The different trends are consistent with the calculated  
477 isochrones, and we consider them as errorchrons. Indeed, the two groups are consistent  
478 according to the field, geochemical and petrological observations.

479 • The O-group includes all the samples that do not spread along calculated isochrones (GDU,  
480 CCU, El Toro, TU, Linga-SJK1 and YU) . The  $^{87}\text{Sr}/^{86}\text{Sr}_i$  range is large (0.70528-0.71228) for a  
481 small range of  $^{87}\text{Rb}/^{86}\text{Sr}_i$  ratio (0.01-1.99). In this group we note the predominance of the mafic  
482 lithologies but also the occurrence of some quartz-diorites and granite.

483 We interpreted the trends obtained for the MP and K groups as errorchrons, as they fit with  
484 the calculated isochrones based on U-Pb zircon ages. According to this interpretation, the  
485 samples that plot along the same line share the same initial isotopic signatures. Then,  
486 variation along the  $^{87}\text{Rb}/^{86}\text{Sr}_i$  axis may be considered at first glance as an effect of fractional  
487 crystallization, as 1) the increase of this ratio is a function of the biotite/plagioclase mineral  
488 cotectic proportions during magma evolution, and of their respective partition coefficients and  
489 2) fractional crystallization alone do not affect the Sr isotopic ratio.

490 The three main groups identified in the Rb-Sr isochron diagram (Figure 9) are reported in  
491 several other plots:  $^{87}\text{Sr}/^{86}\text{Sr}_i$ ,  $^{143}\text{Nd}/^{144}\text{Nd}$  ratios, Lu and Sr concentrations, all plotted versus Zr  
492 concentrations (Figure 11), used as a fractionation index (FC, Pearce and Norry 1979, Figure  
493 D1). Between all the three groups, we can define two general sketches:



494 • The K and MP-groups, which are characterized by a large range of Zr content (96 to 370  
495 ppm), define the same trends. They have narrow ranges of initial  $^{87}\text{Sr}/^{86}\text{Sr}$  (0.70481-0.70594)  
496 and  $^{143}\text{Nd}/^{144}\text{Nd}$  (0.51237-0.51251) isotopic ratio. This is consistent with their respective  
497 position in the Rb-Sr isochron diagram (Figure 7). Relative to Zr, Lu correlates positively, Sr  
498 correlates negatively and initial  $^{87}\text{Sr}/^{86}\text{Sr}$  and  $^{143}\text{Nd}/^{144}\text{Nd}$  ratios remain constant. Therefore, there  
499 is no change in the isotopic signatures during magma differentiation, unlike what is predicted  
500 by AFC.

501 • Data from the O-group are characterized by lower Zr content (<200 ppm) and are much  
502 more scattered compared to the K and MP-groups. The O-group displays large ranges of  
503  $^{87}\text{Sr}/^{86}\text{Sr}$  (0.70388-0.71095) and  $^{143}\text{Nd}/^{144}\text{Nd}$  (0.51202-0.51253) ratios. There is no linear  
504 correlation between the initial isotopic ratios and the fractionation index. Moreover, the  
505 scatter of the data seems to be less pronounced at high Zr abundances. This indicates that the  
506 more the magmas are evolved, the less – trace element content and isotopically speaking -  
507 heterogeneous they are.

508 Considering the entire set of data (MP, K, and O-groups), made of rocks of various ages, we  
509 observe a decrease in the chemical heterogeneity (both isotopic ratios and trace elements)  
510 with the increasing amount of Zr. The samples with Zr content higher than  $\pm 200$  ppm seem to  
511 share similar isotopic source. These features also suggest that different petrological processes  
512 dominate under and above the 200 ppm Zr content threshold.

### 513 7.2.3 Implication for the petrological processes

514 *The MP-group.* The MP-group is comprised of 23 samples, emplaced during a period of 8-  
515 Myr. This group can be described as isotopically homogeneous (Figure 9 and Figure 11).  
516 Processes like AFC, magma mixing/mingling or peritectic inheritance, if any, should have  
517 existed prior to the homogenization of the chemical signatures. As an example, the rocks have  
518 developed highly variable  $^{87}\text{Sr}/^{86}\text{Sr}$  initial isotopic signatures because they were at first  
519 characterized by variable  $^{87}\text{Rb}/^{86}\text{Sr}$  ratios. We propose that this ratio is at first order controlled  
520 by fractional crystallization. The rocks are linked with parental magmas that share common



521 geochemical features, and they underwent similar magmatic histories dominated by fractional  
522 crystallization.

523 The trends defined by the major and trace element data versus Zr abundances are consistent  
524 with this hypothesis, as are the field observations. Indeed, the structural organization of the  
525 Linga unit reveals that it was built as a superposition of several laccolith-shaped intrusions.  
526 This observation rules out the hypothesis that all samples from this group may come from a  
527 single, giant, melt batch that slowly cooled down and fractionated after emplacement. These  
528 laccoliths may then share a single parental magma reservoir that remained hot, stable and  
529 constantly fed at least during 8 Myr.

530 The initial isotopic signatures of this group are therefore the result of an homogenization  
531 process which happened before the replenishment of the parental magmatic reservoir. In this  
532 reservoir, the chemical signatures are neither purely crustal nor juvenile but intermediate.

533 *The O-group.* The O-group displays a broad isotopic, major and trace element heterogeneity.  
534 This heterogeneity tends to decrease as the Zr abundance in the rocks increases. These  
535 features call of several hypothesis concerning the genesis and evolution of the magmas. The  
536 contrasted isotopic signatures, especially for the lowest Zr content rocks, are consistent with  
537 the involvement of both crustal and juvenile sources. The range of isotopic signatures can be  
538 explained by various amounts of mixing between these two end members. We note that the  
539 scatter of the isotopic signatures is not in accordance with an AFC process, considering the  
540 mafic nature of some of the most radiogenic samples. Combined to this mixing process,  
541 fractionation occurs, giving a blend of rock types within the O-group (gabbros to quartz-  
542 diorites).

543 The acquisition of the geochemical heterogeneity is commonly considered to occur at two  
544 levels. Firstly, the source of the magmas may deliver a geochemical fingerprint to the partial  
545 melts. Secondly, the evolution of the magmas through processes like AFC leads to the  
546 dispersion of the initial isotopic ratios. These processes are not mutually exclusive. In our  
547 case, as there is no increase of the scatter in isotopic signatures towards the most evolved  
548 melts, we consider that the AFC process does not dominate the evolution of the magmas. The





549 chemical variability of the mafic end-members reflect the heterogeneity of the source, and the  
550 more the melts fractionated, the less they differ from an isotopic point of view (Voshage et al.,  
551 1990).

552 The initial chemical heterogeneity inherited from the source suggests a gradual  
553 homogenization of the residual magmas as fractionation proceeds, until the melts reach 200  
554 ppm Zr content.

555 *The K-group.* The K-group presents geochemical similarities with the MP-group, especially  
556 in terms of isotopic signatures: initial  $^{87}\text{Sr}/^{86}\text{Sr}$  and  $^{143}\text{Nd}/^{144}\text{Nd}$  ratios are rather consistent within  
557 this group. Fractionation is the primary process that controls the sample signatures within this  
558 group. We note that 4 samples from the K-group are characterized by 100 ppm Zr content,  
559 which is rather low. The [Sr] and [Lu] versus [Zr] content plot (Figure 11) suggest that these  
560 4 samples evolved within an isolated batch, which is consistent with the field data (samples  
561 come from the Linga unit, with ages between 90 -87 Ma, Demouy et al. 2012).

562 Again, despite the various ages and the various plutonic units, there is a consistent scheme  
563 within the geochemical signatures of the samples in the Arequipa area. The first stage ([Zr]  
564 <200 ppm) is dominated by both mixing and fractionation, and the second stage ([Zr] >200  
565 ppm) is mostly dominated by fractionation only, starting from a homogeneous primary  
566 reservoir. Are these assumptions consistent with what we know about the costal Batholith  
567 history?

### 568 *7.3 The evolution of the geochemical signature through time: a geodynamical control?*

569

570 As within several active margins, the magmatic activity in the margin of Southern Peru is  
571 discontinuous during the Mesozoic and the Cenozoic (Dallmeyer et al., 1996; Coleman and  
572 Glazner, 1997; Ducea, 2001; Lucassen et al., 2002; Parada et al., 2005; DeCelles et al., 2009;  
573 Demouy et al., 2012). The emplacement of the plutonic rocks through time is a record of the  
574 magmatic arc localization, alternatively trenchward and landward (Mamani et al., 2008;  
575 Demouy et al., 2012). This movement is linked to the global geodynamic context: from at  
576 least the late Permian, the active margin of Southern Peru is experiencing an extensive regime.



577 This leads to an important crustal thinning that started in the Early Jurassic and culminated in  
578 the Middle Jurassic (Sempere et al., 2002). The arc migrates trenchward from 200 to at least  
579 150 Ma. This extension stops during the Early Cretaceous before westward drifting after the  
580 Cenomanian (Somoza and Zaffarana, 2008). During this period, the arc migrates landward  
581 and impinged the Arequipa area from 90 to at least 60 Ma.

582 Plate tectonic considerations have strong implications for the magma genesis and  
583 emplacement in this specific geodynamic environment. Considering the theoretical MASH  
584 model (Hildreth and Moorbath, 1988) and its recent support through numerical models  
585 (Annen et al., 2006b), we suggest that deep crustal hot zones are areas where the geochemical  
586 signatures of the magmas are acquired. Several studies attest that the accumulation of silicic  
587 magmas in a relatively cold and brittle environment favors eruption over accumulation, while  
588 later magmas accumulation in a warm ductile crust favors accumulation over eruption  
589 (Jellinek and DePaolo, 2003; de Silva et al., 2006a and b; Bachmann et al., 2007).

590 In the Arequipa area we identify two contrasted tectonic contexts during the magmatic arc  
591 activity in Arequipa: (i) initiation and protracted magmatic activity within a thinned Jurassic  
592 crust (200-175 Ma) (ii) initiation and protracted magmatic activity within a thickening crust,  
593 from the Late Cretaceous to the Maastrichtian-Paleocene (90-60 Ma).

594 We can link the geochemical groups (O-K-and MP-) with these two situations. The O-group  
595 is mainly composed of Jurassic rocks and some of the oldest Cretaceous rocks of Linga and  
596 the Tiabaya unit. It corresponds to stage (i) and part of stage (ii). The O-group melts did not  
597 evolve in a thickened crust. The K-group and MP-group correspond to the protracted activity  
598 of stage (ii), i.e. the evolution of the magmatic activity within a hot crust being thicken.

599 The initiation of magmatic activity at the base of the crust may trigger the emplacement of a  
600 certain amount of juvenile magma around the crust/mantle boundary. These magmas quickly  
601 crystallize at first, but the gradual heating of the deep crustal hot zone allows the production  
602 of various magma batches, characterized by various amounts of crustal input. This stage  
603 corresponds to the Mixing and Assimilation processes from the MASH model. In Arequipa,  
604 the Jurassic magmas (Gabbros & Diorites, El Toro and Chapi-Churajón plutons) are



605 characterized by large geochemical heterogeneities, especially in the isotopic signal. Plutonic  
606 bodies are relatively small compared to the Jurassic volcanic and volcanoclastic deposits in  
607 Southern Peru (up to 6 km-thick, Chocolate Formation, Boekhout et al. 2013). The protracted  
608 magmatic activity from 200 to 175 Ma in Arequipa was not sufficient to thicken the crustal  
609 arc section, as the active margin was subject to an important crustal thinning during this  
610 period (Sempere et al., 2002). Hence, the crust do not reach a mature thermal state, but the  
611 gradual heating of the deep crust system still triggered partial homogenization of the magmas  
612 (O-group between 0 and 200 ppm Zr content). The petrological processes that dominate in  
613 this case are mixing and fractional crystallization.

614 Around 90 Ma, the reactivation of the magmatic activity below a cold crust leads to similar  
615 plutonic body emplacements: they are small in size and do present contrasted isotopic  
616 signatures (Linga-SJK1 and Tiabaya groups). These characteristics then changed. The active  
617 margin is no longer under extensional regime, allowing the thickening of the crust below the  
618 magmatic arc. This thickening leads to the development of a deep hot crustal zone that  
619 reaches a "mature" thermal state. This situation favors magma storage and homogenization at  
620 great depth, from a simple buoyancy point of view. Numerical models attest that silica-rich  
621 magmas can be generated by incomplete crystallization of hydrous basalts in the deep crust  
622 (Müntener et al., 2001; Prouteau and Scaillet, 2003). Hence the thermal maturation of the arc  
623 system allows the generation of more differentiated magmas that are submitted to Storage and  
624 Homogenization (MASH model). This evolution leads to the emplacement of large plutonic  
625 bodies at the batholith level, which are mainly subject to magmatic fractionation. These  
626 bodies are sharing common primitive parental melts, located at a deep level in a single,  
627 homogeneous, reservoir (K-and MP-group). The MP-group is symptomatic of this system:  
628 from 70 to 60 Ma, thousands of km<sup>3</sup> of magmatic liquids are produced, all sharing the same  
629 source; it is defined as a flare-up event. It is worth noting that this period is characterized by  
630 large ignimbritic explosions at the surface, which may be intrinsically linked to this process  
631 (in Southern Peru, Paralaque Formation, Bellido and Guevara 1963; Martinez and Cervantes  
632 2003).

633    **8. CONCLUSIONS**

634    The Arequipa batholith is made up of several plutonic units that record a long subduction-  
635    related discontinuous magmatic activity from the Jurassic to the Paleocene (200-175 and 90-  
636    60 Ma). The various plutonic units display a large geochemical heterogeneity at the batholith  
637    scale that are consistent with the signatures reported for plutonic rocks in magmatic arcs. Both  
638    field observations and barometric calculations obtained on amphibole phases allow to identify  
639    several vertical movements during the batholith emplacement, especially linked to the main  
640    Lluçla Fault System. The Jurassic rocks from the Gabbros & Diorites unit emplaced at  
641    shallow depth (0.8 kb in average), before being buried under a thick sedimentary cover during  
642    the crustal thinning affecting the entire active margin of Southern Peru. The reactivation of  
643    the magmatic activity during the Late Cretaceous leads to the emplacement of plutonic rocks  
644    at two different levels: the Tiabaya unit emplaced through the Gabbros & Diorites unit at a  
645    deeper level ( 5-7 km depth) than the Linga unit ( 3.5 km depth). These two plutonic units are  
646    currently located at the same elevation and are separated by the Lluçla Fault System. We  
647    propose that this Fault System activation leads to the raising of the Tiabaya unit between 76  
648    and 68 Ma. This is confirmed by the fact that Maastrichtian-Paleocene rocks cropping out on  
649    both sides of the Lluçla Fault System display the same amphibole crystallization pressure.

650    The geochemical signatures of the plutonic rocks of the Arequipa batholith display a large  
651    heterogeneity within the mafic samples, and we observe a tendency for homogenization  
652    linked to fractionation. We propose a two-stage evolution model for the magmatic arc in the  
653    Arequipa area. The first stage consists in the initiation of the magmatic activity that leads to  
654    the emplacement of disconnected, mafic, small and isotopically heterogeneous plutons. This  
655    stage is due to the domination of mixing and fractional crystallization petrological processes  
656    in the deep crust, and lasts as long as the crustal arc section cannot thicken and reach a  
657    thermal maturity threshold. In Arequipa, the crustal thinning that occurs during the Jurassic  
658    period prevents from reaching this maturity. The switch to a convergent geodynamical  
659    context from the Early Cretaceous allows the thickening of the arc crust section. The second  
660    stage is reached when the crust has thickened enough to allow the development of a deep hot



661 crustal zone where the petrological processes of homogenization and fractional crystallization  
662 are dominant. During this second stage, the softening of the crust at several levels allows the  
663 formation of deep magmatic reservoirs from which numerous magmas batches rise to emplace  
664 as voluminous plutons at the batholith level. The paroxysm of this system leads to the  
665 occurrence of flare-up events, and to the concomitant emplacement of the largest plutonic  
666 units and major ignimbritic explosions.

## 667 FUNDING

668 The project was supported by the Institut de Recherche pour le Développement and the  
669 Institut National des Sciences de l'Univers - CNRS SYSTER program.

670

## 671 ACKNOWLEDGEMENTS

672 We thank Georges Ceuleneer for his careful rereading, Pierre Brunet, Jonathan Prunier and  
673 Manuel Henry for the technical assistance. The Sociedad Minera Cerro Verde S.A.A has  
674 allowed a significant part of the field studies.

## 675 REFERENCES

- 676 Anders, E. and Grevesse, N.: Abundances of the elements: meteoric and solar. *Geochimica et*  
677 *Cosmochimica Acta* 53: 197-214, 1989.
- 678 Annen, C., Blundy, J. D. and Sparks, R. S. J.: The Genesis of Intermediate and Silicic  
679 Magmas in Deep Crustal Hot Zones, *J Petrology*, 47(3), 505–539,  
680 doi:10.1093/petrology/egi084, 2006.
- 681 Atherton, M. and Petford, N.: Generation of Sodium-Rich Magmas from Newly Underplated  
682 Basaltic Crust, *Nature*, 362(6416), 144–146, doi:10.1038/362144a0, 1993.
- 683 Bachmann, O., Miller, C. F. and de Silva, S. L.: The volcanic-plutonic connection as a stage  
684 for understanding crustal magmatism, *J. Volcanol. Geotherm. Res.*, 167(1–4), 1–23,  
685 doi:10.1016/j.jvolgeores.2007.08.002, 2007.
- 686 Bartley, J. M., Coleman, D. S. and Glazner, A. F.: Incremental pluton emplacement by  
687 magmatic crack-seal, *Trans. R. Soc. Edinb.-Earth Sci.*, 97, 383–396,  
688 doi:10.1017/S0263593300001528, 2006.
- 689 Beck, S. L., Zandt, G., Myers, S. C., Wallace, T. C., Silver, P. G. and Drake, L.: Crustal-  
690 thickness variations in the central Andes, *Geology*, 24(5), 407–410, doi:10.1130/0091-  
691 7613(1996)024<0407:CTVITC>2.3.CO;2, 1996.



- 692 Bel, L.: Mineralization in the Arequipa segment: the porphyry-Cu deposit of Cerro  
693 Verde/Santa Rosa., in Magmatism at a plate edge. The Peruvian Andes, Blackie Halsted Press,  
694 Glasgow and London., 1985.
- 695 Bellido Bravo, E. and Guevara Rosillo, C.: Geología de los cuadrángulos de Punta de  
696 Bombón y Cledesí 35-s y 35-t - [Boletín A 5], Instituto Geológico, Minero y Metalúrgico.  
697 1963.
- 698 Boekhout, F., Sempere, T., Spikings, R. and Schaltegger, U.: Late Paleozoic to Jurassic  
699 chronostratigraphy of coastal southern Peru: Temporal evolution of sedimentation along an  
700 active margin, *J. South Am. Earth Sci.*, 47, 179–200, doi:10.1016/j.jsames.2013.07.003, 2013.
- 701 Boily, M., Brooks, C., Ludden, J. and James, D.: Chemical and Isotopic Evolution of the  
702 Coastal Batholith of Southern Peru, *Journal of Geophysical Research-Solid Earth and Planets*,  
703 94(B9), 12483–12498, doi:10.1029/JB094iB09p12483, 1989.
- 704 Casquet, C., Fanning, C. M., Galindo, C., Pankhurst, R. J., Rapela, C. W. and Torres, P.: The  
705 Arequipa Massif of Peru: New SHRIMP and isotope constraints on a Paleoproterozoic inlier  
706 in the Grenvillian orogen, *J. South Am. Earth Sci.*, 29(1), 128–142,  
707 doi:10.1016/j.jsames.2009.08.009, 2010.
- 708 Cawood, P. A.: Terra Australis Orogen: Rodinia breakup and development of the Pacific and  
709 Iapetus margins of Gondwana during the Neoproterozoic and Paleozoic, *Earth-Sci. Rev.*,  
710 69(3–4), 249–279, doi:10.1016/j.earscirev.2004.09.001, 2005.
- 711 Clemens, J. D. and Stevens, G.: What controls chemical variation in granitic magmas?, *Lithos*,  
712 134, 317–329, doi:10.1016/j.lithos.2012.01.001, 2012.
- 713 Clemens, J. D., Darbyshire, D. P. F. and Flinders, J.: Sources of post-orogenic calcalkaline  
714 magmas: The Arrochar and Garabal Hill-Glen Fyne complexes, Scotland, *Lithos*, 112(3–4),  
715 524–542, doi:10.1016/j.lithos.2009.03.026, 2009.
- 716 Clemens, J. D., Helps, P. A. and Stevens, G.: Chemical structure in granitic magmas - a signal  
717 from the source?, *Earth Environ. Sci. Trans. R. Soc. Edinb.*, 100, 159–172,  
718 doi:10.1017/S1755691009016053, 2010.
- 719 Coleman, D. S. and Glazner, A. F.: The Sierra Crest magmatic event: Rapid formation of  
720 juvenile crust during the Late Cretaceous in California, edited by W. G. Ernst and C. A.  
721 Nelson, Bellwether Publishing, Ltd, Columbia, 1998.
- 722 Cox, K. G., Bell, J. D. and Pankhurst, R. J.: The interpretation of igneous rocks, 1st ed., repr.,  
723 Chapman & Hall, London., 1993.
- 724 Cruden, A. R. and McCaffrey, K. J. W.: Growth of plutons by floor subsidence: Implications  
725 for rates of emplacement, intrusion spacing and melt-extraction mechanisms, *Phys. Chem.*  
726 *Earth Pt. A-Solid Earth Geod.*, 26(4–5), 303–315, doi:10.1016/S1464-1895(01)00060-6, 2001.
- 727 Cruz, M.: Estratigrafía y evolución tectono-sedimentaria de los depósitos sin-orogénicos del  
728 cuadrángulo de Huambo (32-r, Cuadrante-II): Las formaciones Ashua y Huanca.  
729 Departamento de Arequipa, PhD, Universidad Nacional San Agustín de Arequipa., 2002.
- 730 Dallmeyer, R. D., Brown, M., Grocott, J., Taylor, G. K. and Treloar, P. J.: Mesozoic  
731 magmatic and tectonic events within the Andean plate boundary zone, 26 degrees-27 degrees  
732 30'S, North Chile: Constraints from Ar-40/Ar-39 mineral ages, *J. Geol.*, 104(1), 19–40,  
733 doi:10.1086/629799, 1996.
- 734 De Silva, S., Silva, S. D., Zandt, G., Trumbull, R., Viramonte, J. G., Salas, G. and Jimenez,  
735 N.: Large ignimbrite eruptions and volcano-tectonic depressions in the Central Andes: a



- 736 thermomechanical perspective, Geological Society, London, Special Publications, 269(1), 47–  
737 63, n.d.
- 738 DeCelles, P. G., Ducea, M. N., Kapp, P. and Zandt, G.: Cyclicity in Cordilleran orogenic  
739 systems, *Nat. Geosci.*, 2(4), 251–257, doi:10.1038/NGEO469, 2009.
- 740 Demouy, S.: La naissance des Andes au Crétacé supérieur: origine et construction du  
741 Batholite Côtier sud-péruvien (Région d'Arequipa), Thèse d'Université, Université Paul  
742 Sabatier, Toulouse, 2012.
- 743 Demouy, S., Paquette, J.-L., de Saint Blanquat, M., Benoit, M., Belousova, E. A., O'Reilly, S.  
744 Y., Garcia, F., Tejada, L. C., Gallegos, R. and Sempere, T.: Spatial and temporal evolution of  
745 Liassic to Paleocene arc activity in southern Peru unraveled by zircon U-Pb and Hf in-situ  
746 data on plutonic rocks, *Lithos*, 155, 183–200, doi:10.1016/j.lithos.2012.09.001, 2012.
- 747 DePaolo, D. J.: A neodymium and strontium isotopic study of the Mesozoic calc-alkaline  
748 granitic batholiths of the Sierra Nevada and Peninsular Ranges, California, *Journal of*  
749 *Geophysical Research: Solid Earth*, 86(B11), 10470–10488, doi:10.1029/JB086iB11p10470,  
750 1981.
- 751 Ducea, M.: The California Arc: Thick Granitic Batholiths, Eclogitic Residues, Lithospheric-  
752 Scale Thrusting, and Magmatic Flare-Ups, *GSA TODAY*, 7, 2001.
- 753 Ducea, M. N. and Barton, M. D.: Igniting flare-up events in Cordilleran arcs, *Geology*, 35(11),  
754 1047–1050, doi:10.1130/G23898A.1, 2007.
- 755 Dungan, M. A. and Davidson, J.: Partial assimilative recycling of the mafic plutonic roots of  
756 arc volcanoes: An example from the Chilean Andes, *Geology*, 32(9), 773–776,  
757 doi:10.1130/G20735.1, 2004.
- 758 Ganne, J., Schellart, W., Rosenbaum, G., Feng, X. and de Andrade, V.: Probing crustal  
759 thickness evolution and geodynamic processes in the past from magma records: An integrated  
760 approach, *GSA Special Paper*, 526, DOI :10.1130/2017.2526(01), 2017.
- 761 Glazner, A. F.: Thermal limitations on incorporation of wall rock into magma, *Geology*, 35(4),  
762 319–322, doi:10.1130/G23134A.1, 2007.
- 764 Grove, T. L., Parman, S. W., Bowring, S. A., Price, R. C. and Baker, M. B.: The role of an  
765 H<sub>2</sub>O-rich fluid component in the generation of primitive basaltic andesites and andesites from  
766 the Mt. Shasta region, N California, *Contrib. Mineral. Petrol.*, 142(4), 375–396,  
767 doi:10.1007/s004100100299, 2002.
- 768 Grove, T. L., Elkins-Tanton, L. T., Parman, S. W., Chatterjee, N., Muntener, O. and Gaetani,  
769 G. A.: Fractional crystallization and mantle-melting controls on calc-alkaline differentiation  
770 trends, *Contrib. Mineral. Petrol.*, 145(5), 515–533, doi:10.1007/s00410-003-0448-z, 2003.
- 771 Hamilton, W.: Orogenic Andesites and Plate-Tectonics - Gill, Jb, *Am. J. Sci.*, 283(6), 633–634,  
772 1983.
- 773 Haschke, M., Siebel, W., Gunther, A. and Scheuber, E.: Repeated crustal thickening and  
774 recycling during the Andean orogeny in north Chile (21 degrees–26 degrees S), *J. Geophys.*  
775 *Res.-Solid Earth*, 107(B1), 3019, doi:10.1029/2001JB000328, 2002.
- 776 Herve, F., Pankhurst, R. J., Fanning, C. M., Calderon, M. and Yaxley, G. M.: The South  
777 Patagonian batholith: 150 my of granite magmatism on a plate margin, *Lithos*, 97(3–4), 373–  
778 394, doi:10.1016/j.lithos.2007.01.007, 2007.





- 779 Hildreth, W. and Moor bath, S.: Crustal Contributions to Arc Magmatism in the Andes of  
780 Central Chile, *Contrib. Mineral. Petrol.*, 98(4), 455–489, doi:10.1007/BF00372365, 1988.
- 781 James, D. E.: Andean crustal and upper mantle structure, *Journal of Geophysical Research*  
782 (1896–1977), 76(14), 3246–3271, doi:10.1029/JB076i014p03246, 1971.
- 783 Jellinek, A. M. and DePaolo, D. J.: A model for the origin of large silicic magma chambers:  
784 precursors of caldera-forming eruptions, *Bull. Volcanol.*, 65(5), 363–381,  
785 doi:10.1007/s00445-003-0277-y, 2003.
- 786 Le Bel, L.: Mineralization in the Arequipa segment: the porphyry-Cu deposit of Cerro  
787 Verde/Santa Rosa, edited by Pitcher W.S., Atherton M.P., Cobbing E.J. et Beckinsale E.R.D.,  
788 Magmatism at a plate edge, The Peruvian Andes, Blackie Halsted Press, Glasgow and  
789 London, 1985.
- 790 Leuthold, J., Muentener, O., Baumgartner, L. P., Putlitz, B., Ovtcharova, M. and Schaltegger,  
791 U.: Time resolved construction of a bimodal laccolith (Torres del Paine, Patagonia), *Earth*  
792 *Planet. Sci. Lett.*, 325, 85–92, doi:10.1016/j.epsl.2012.01.032, 2012.
- 793 Loewy, S. L., Connelly, J. N. and Dalziel, I. W. D.: An orphaned basement block: The  
794 Arequipa-Antofalla basement of the central Andean margin of South America, *Geol. Soc. Am.*  
795 *Bull.*, 116(1–2), 171–187, doi:10.1130/B25226, 2004.
- 796 Lucassen, F., Escayola, M., Romer, R. L., Viramonte, J., Koch, K. and Franz, G.: Isotopic  
797 composition of Late Mesozoic basic and ultrabasic rocks from the Andes (23–32°S) –  
798 implications for the Andean mantle, *Contrib Mineral Petrol.*, 143(3), 336–349,  
799 doi:10.1007/s00410-001-0344-3, 2002.
- 800 Mamani, M., Tassara, A. and Woerner, G.: Composition and structural control of crustal  
801 domains in the central Andes, *Geochem. Geophys. Geosyst.*, 9, Q03006,  
802 doi:10.1029/2007GC001925, 2008.
- 803 Mamani, M., Woerner, G. and Sempere, T.: Geochemical variations in igneous rocks of the  
804 Central Andean orocline (13 degrees S to 18 degrees S): Tracing crustal thickening and  
805 magma generation through time and space, *Geol. Soc. Am. Bull.*, 122(1–2), 162–182,  
806 doi:10.1130/B26538.1, 2010.
- 807 Martignole, J. and Martelat, J. E.: Regional-scale Grenvillian-age UHT metamorphism in the  
808 Mollendo-Camana Block (basement of the Peruvian Andes), *J. Metamorph. Geol.*, 21(1), 99–  
809 120, doi:10.1046/j.1525-1314.2003.00417.x, 2003.
- 810 Matzel, J. E. P., Bowring, S. A. and Miller, R. B.: Time scales of pluton construction at  
811 differing crustal levels: Examples from the Mount Stuart and Tenpeak intrusions, North  
812 Cascades, Washington, *Geol. Soc. Am. Bull.*, 118(11–12), 1412–1430, doi:10.1130/B25923.1,  
813 2006.
- 814 McCulloch, M. and Gamble, J.: Geochemical and Geodynamical Constraints on Subduction  
815 Zone Magmatism, *Earth Planet. Sci. Lett.*, 102(3–4), 358–374, doi:10.1016/0012-  
816 821X(91)90029-H, 1991.
- 817 Miller, C. F., Furbish, D. J., Walker, B. A., Claiborne, L. L., Koteas, G. C., Bleick, H. A. and  
818 Miller, J. S.: Growth of plutons by incremental emplacement of sheets in crystal-rich host:  
819 Evidence from Miocene intrusions of the Colorado River region, Nevada, USA,  
820 *Tectonophysics*, 500(1–4), 65–77, doi:10.1016/j.tecto.2009.07.011, 2011.
- 821 Miskovic, A., Spikings, R. A., Chew, D. M., Kosler, J., Ulianov, A. and Schaltegger, U.:  
822 Tectonomagmatic evolution of Western Amazonia: Geochemical characterization and zircon  
823 U-Pb geochronologic constraints from the Peruvian Eastern Cordilleran granitoids, *Geol. Soc.*





- 824 Am. Bull., 121(9–10), 1298–1324, doi:10.1130/B26488.1, 2009.
- 825 Mukasa, S.: Common Pb Isotopic Compositions of the Lima, Arequipa and Toquepala  
826 Segments in the Coastal Batholith, Peru - Implications for Magmagenesis, *Geochim.*  
827 *Cosmochim. Acta*, 50(5), 771–782, doi:10.1016/0016-7037(86)90353-4, 1986a.
- 828 Mukasa, S.: Zircon U-Pb Ages of Super-Units in the Coastal Batholith, Peru - Implications  
829 for Magmatic and Tectonic Processes, *Geol. Soc. Am. Bull.*, 97(2), 241–254,  
830 doi:10.1130/0016-7606(1986)97<241:ZUAOSI>2.0.CO;2, 1986b.
- 831 Muntener, O., Kelemen, P. B. and Grove, T. L.: The role of H<sub>2</sub>O during crystallization of  
832 primitive arc magmas under uppermost mantle conditions and genesis of igneous pyroxenites:  
833 an experimental study, *Contrib. Mineral. Petrol.*, 141(6), 643–658, 2001.
- 834 Pankhurst, R. J.: W. S. Pitcher, M. P. Atherton, E. J. Cobbing and R. D. Beckinsale., eds.  
835 *Magmatism at a Plate Edge: the Peruvian Andes*. Glasgow (Blackie) and New York (Halsted  
836 Press), 1985. x + 328 pp., 246 figs., 2 coloured geological maps. Price £65, *Mineralogical*  
837 *Magazine*, 50(356), 351–351, doi:10.1180/minmag.1986.050.356.30, 1986.
- 838 Parada, M., Lopez-Escobar, L., Oliveros, V., Fuentes, F. and Morata, D.: Andean  
839 Magmatism., in *The Geology of Chile*, pp. 115–146, The Geological Society of London., n.d.
- 840 Parada, M. A., Feraud, G., Fuentes, F., Aguirre, L., Morata, D. and Larrondo, P.: Ages and  
841 cooling history of the Early Cretaceous Caleu pluton: testimony of a switch from a rifted to a  
842 compressional continental margin in central Chile, *J. Geol. Soc.*, 162, 273–287,  
843 doi:10.1144/0016-764903-173, 2005.
- 844 Pearce, J. and Norry, M.: Petrogenetic Implications of Ti, Zr, Y, and Nb Variations in  
845 Volcanic-Rocks, *Contrib. Mineral. Petrol.*, 69(1), 33–47, doi:10.1007/BF00375192, 1979.
- 846 Powell, R.: Inversion of the Assimilation and Fractional Crystallization (afc) Equations -  
847 Characterization of Contaminants from Isotope and Trace-Element Relationships in Volcanic  
848 Suites, *J. Geol. Soc.*, 141(MAY), 447–452, doi:10.1144/gsjgs.141.3.0447, 1984.
- 849 Prouteau, G. and Scaillet, B.: Experimental constraints on the origin of the 1991 Pinatubo  
850 dacite, *J. Petrol.*, 44(12), 2203–2241, doi:10.1093/petrology/egg075, 2003.
- 851 Rapp, R.: Amphibole-Out Phase-Boundary in Partially Melted Metabasalt, Its Control Over  
852 Liquid Fraction and Composition, and Source Permeability, *J. Geophys. Res.-Solid Earth*,  
853 100(B8), 15601–15610, doi:10.1029/95JB00913, 1995a.
- 854 Rapp, R. P.: Amphibole-out phase boundary in partially melted metabasalt, its control over  
855 liquid fraction and composition, and source permeability, *Journal of Geophysical Research:*  
856 *Solid Earth*, 100(B8), 15601–15610, doi:10.1029/95JB00913, 1995b.
- 857 Ridolfi, F. and Renzulli, A.: Calcic amphiboles in calc-alkaline and alkaline magmas:  
858 thermobarometric and chemometric empirical equations valid up to 1,130°C and 2.2 GPa,  
859 *Contributions to Mineralogy and Petrology*, 163, 877–895, doi:10.1007/s00410-011-0704-6,  
860 2012.
- 861 de Saint Blanquat, M., Horsman, E., Habert, G., Morgan, S., Vanderhaeghe, O., Law, R. and  
862 Tikoff, B.: Multiscale magmatic cyclicity, duration of pluton construction, and the  
863 paradoxical relationship between tectonism and plutonism in continental arcs, *Tectonophysics*,  
864 500(1–4), 20–33, doi:10.1016/j.tecto.2009.12.009, 2011.
- 865 de Saint-Blanquat, M., Law, R. D., Bouchez, J. L. and Morgan, S. S.: Internal structure and  
866 emplacement of the Papoose Flat pluton: An integrated structural, petrographic, and magnetic  
867 susceptibility study, *Geol. Soc. Am. Bull.*, 113(8), 976–995, doi:10.1130/0016-



- 868 7606(2001)113<0976:ISAEOT>2.0.CO;2, 2001.
- 869 Sempere, T., Carlier, G., Soler, P., Fornari, M., Carlotto, V., Jacay, J., Arispe, O., Neraudeau,  
870 D., Cardenas, J., Rosas, S. and Jimenez, N.: Late Permian-Middle Jurassic lithospheric  
871 thinning in Peru and Bolivia, and its bearing on Andean-age tectonics, *Tectonophysics*,  
872 345(1–4), 153–181, doi:10.1016/S0040-1951(01)00211-6, 2002.
- 873 Shackleton, R.M., Ries, A.C., Coward, M.P., Cobbold, P.R.: Structure, metamorphism and  
874 geochronology of the Arequipa Massif of coastal Peru, *Journal of the Geological Society*, 136,  
875 195–214, 1979.
- 876 Sisson, T. and Layne, G.: H<sub>2</sub>O in Basalt and Basaltic Andesite Glass Inclusions from 4  
877 Subduction-Related Volcanos, *Earth Planet. Sci. Lett.*, 117(3–4), 619–635, doi:10.1016/0012-  
878 821X(93)90107-K, 1993.
- 879 Smith, A. L., Schellekens, J. H. and Díaz, A.-L. M.: Batholiths as markers of tectonic change  
880 in the northeastern Caribbean, in *Special Paper 322: Tectonics and Geochemistry of the*  
881 *Northeastern Caribbean*, vol. 322, pp. 99–122, Geological Society of America., 1998.
- 882 Somoza, R. and Zaffarana, C. B.: Mid-Cretaceous polar standstill of South America, motion  
883 of the Atlantic hotspots and the birth of the Andean cordillera, *Earth Planet. Sci. Lett.*, 271(1–  
884 4), 267–277, doi:10.1016/j.epsl.2008.04.004, 2008.
- 885 Spera, F. J. and Bohrsen, W. A.: Energy-constrained open-system magmatic processes I:  
886 General model and energy-constrained assimilation and fractional crystallization (EC-AFC)  
887 formulation, *J. Petrol.*, 42(5), 999–1018, doi:10.1093/petrology/42.5.999, 2001.
- 888 Stewart, J. W.: *Geología - Cuadrangulo de Mollendo (34r) y La Joya (34s)*, calameo.com  
889 [online] Available from: <https://www.calameo.com/books/0008201299ceeee304f7d>  
890 (Accessed 28 February 2019), 1968.
- 891 Sun, S. -s. and McDonough, W. F.: Chemical and isotopic systematics of oceanic basalts:  
892 implications for mantle composition and processes, *Geological Society, London, Special*  
893 *Publications*, 42(1), 313–345, doi:10.1144/GSL.SP.1989.042.01.19, 1989.
- 894 Tepper, J. H., Nelson, B. K., Bergantz, G. W. and Irving, A. J.: Petrology of the Chilliwack  
895 batholith, North Cascades, Washington: generation of calc-alkaline granitoids by melting of  
896 mafic lower crust with variable water fugacity, *Contr. Mineral. and Petrol.*, 113(3), 333–351,  
897 doi:10.1007/BF00286926, 1993.
- 898 Tilton, G. and Barreiro, B.: Origin of Lead in Andean Calc-Alkaline Lavas, Southern Peru,  
899 *Science*, 210(4475), 1245–1247, doi:10.1126/science.210.4475.1245, 1980.
- 900 Voshage, H., Hofmann, A., Mazzucchelli, M., Rivalenti, G., Sinigoi, S., Raczek, I. and  
901 Demarchi, G.: Isotopic Evidence from the Ivrea Zone for a Hybrid Lower Crust Formed by  
902 Magmatic Underplating, *Nature*, 347(6295), 731–736, doi:10.1038/347731a0, 1990.

903

904 TABLE CAPTION

905 Table 1: Characteristics of the main mineral phases encountered in the Arequipa batholith.

906 FIGURE CAPTIONS



907 Figure 1: Geological map of the Coastal Batholith section in the Arequipa vicinity. ASF:  
908 Agua Salada Fault; LFS: Lluclla Fault System; CF: Cenicienta Fault.

909 Figure 2: Photomicrographs of thin sections (a) Small rounded pyroxenes in a plagioclase  
910 matrix (09SD43); (b) Residual pyroxene cores in amphibole grain (09SD33)

911 Figure 3: a) Amphibole compositions. Na+K (afpu) content vs. Si (afpu) diagram. The  
912 chemical data define two trends; amphiboles from the Gabbro and Diorites and Tiabaya units  
913 define the less Si-enriched trend and amphiboles from the Linga and Yarabamba units define  
914 the more Si-enriched trend. This highlights the general depletion in Si and alkaline in the  
915 amphibole spectrum. (GDU: Gabbros and Diorites unit, TU: Tiabaya unit, LU: Linga unit,  
916 YU : Yarabamba unit). b) Biotite compositions. Al (afpu) content vs. XMg diagram. We  
917 observe an unequal distribution of the biotites in the diagram with two groups, non-linked to  
918 the rock types. The distribution is correlated with the location of the sample; biotites with Al  
919 (afpu)>2.5 belong the Gabbro and Diorite unit and Tiabaya units, whereas biotites with Al  
920 (afpu)<2.5 belong to the Linga and Yarabamba units.

921 Figure 4: Pressure vs. temperature binary diagram for thermobarometric data issue from the  
922 analysis of amphiboles from the Arequipa batholith. G&D.U: Gabbros and Diorites unit, T.  
923 U: Tiabaya unit, L. U: Linga unit, Y. U : Yarabamba unit. BST: basement sample.

924 Figure 5: a) Total alkali vs Silica diagram for the rocks of the Arequipa's batholith. Blue  
925 diamonds: Jurassic rocks; green squares: Cretaceous rocks; orange triangles: Maastrichtian-  
926 Paleocene rocks. Domains from Cox et al. (1979). b) AFM diagram. Blue symbols: Jurassic  
927 rocks; green symbols: cretaceous rocks; orange symbols: maastrichtian-paleocene rocks. c)  
928 A/NK vs. A/CNK diagram. Blue symbols: Jurassic rocks; green symbols: cretaceous rocks;  
929 orange symbols: maastrichtian-paleocene rocks.

930 Figure 6: a) Chondrites normalized REE patterns of the plutonic rocks of the Arequipa  
931 batholith for the different facies (Anders & Grevesse, 1989). The domain of the Andean rocks  
932 is indicated in grey. b) Trace element spider diagram for the plutonic rocks of the Arequipa  
933 batholith (Sun & McDonough, 1989). The domain of the Andean rocks is indicated in grey.



934 Figure 7: Rb-Sr isochron diagram for the plutonic rocks of the Arequipa batholith. Symbols  
935 are the same as in figure 4.

936 Figure 8: Sm-Nd isochron diagram for the plutonic rocks of the Arequipa batholith. Symbols  
937 are the same as in figure 4.

938 Figure 9:  $\epsilon\text{Nd}$  values vs.  $^{87}\text{Sr}/^{86}\text{Sr}_i$  ratios for the plutonic rocks of the Arequipa batholith.  
939 Symbols are the same as in figure 4.

940 Figure 10: Schematic cross section of the northwestern area of the Arequipa Batholith. LFS:  
941 Lluçlla Fault System, CF: Cenicienta Fault, ASF: Aguasalada fault. The LFS separates the  
942 batholith into two parts: (i) a northeastern part made of the Gabbros & Diorites unit, the  
943 Tiabaya unit, the precambrian basement and the Early Jurassic sedimentary strata (b) a  
944 southwestern part made up of the large Linga unit made of an amalgamation of several  
945 laccolith shaped intrusions crosscutting the Jurassic sedimentary strata.

946 Figure 11:  $^{87}\text{Sr}/^{86}\text{Sr}_i$ ,  $^{143}\text{Nd}/^{144}\text{Nd}_i$  ratios, Lu and Sr concentrations, all plotted versus Zr  
947 concentrations.

948

949 Supplementary files:

950 Supplement A: Coordinates of the 100 samples issued from the Arequipa section of the  
951 Southern Coastal batholith of Peru

952 Supplement B: Thermobarometric data for selected samples from the Arequipa batholith.  
953 Calculations based on the model from Ridolfi and Renzulli (2012).

954 Supplement C: Major and trace elements for 100 samples issued from the Arequipa batholith  
955 section.

956 Supplement D: Isotopic data and Rb, Sr, Sm, Nd abundances for selected samples from the  
957 Arequipa batholith section.

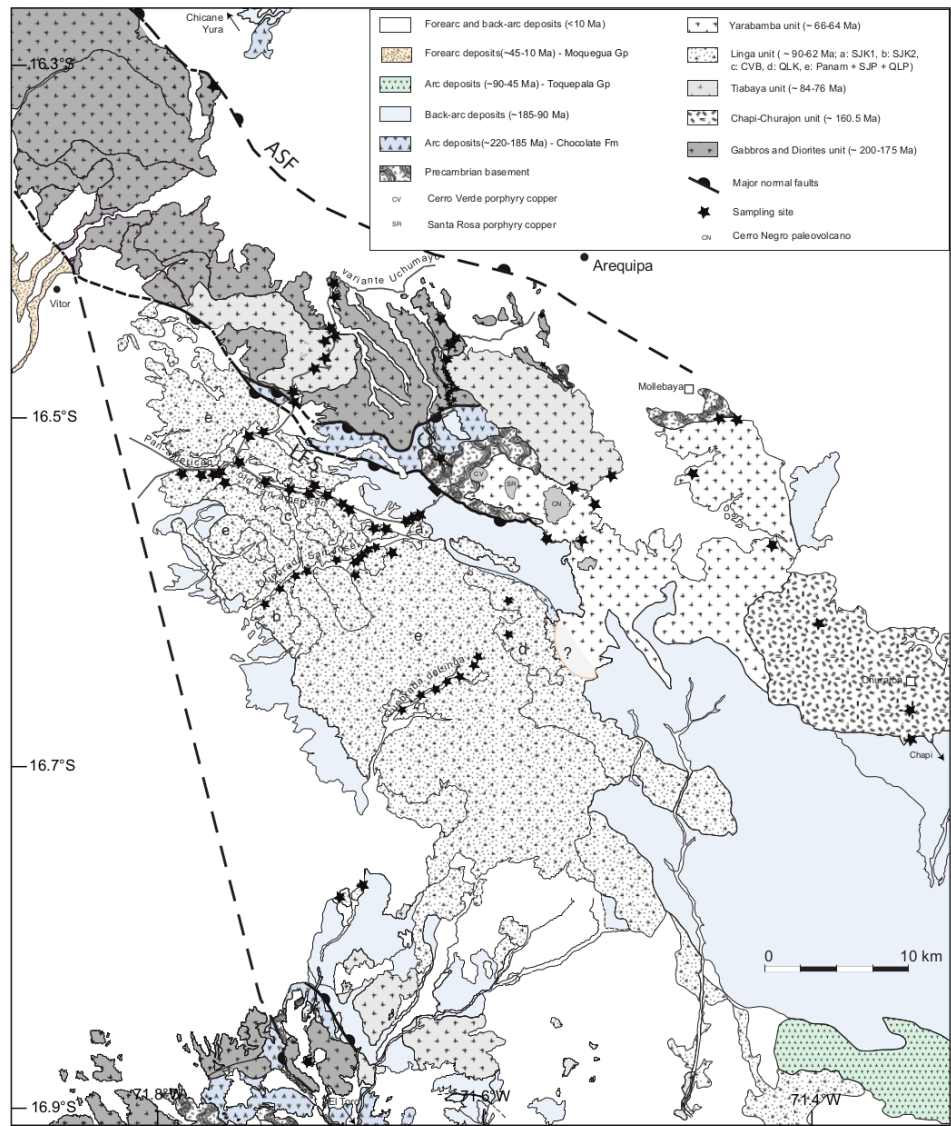
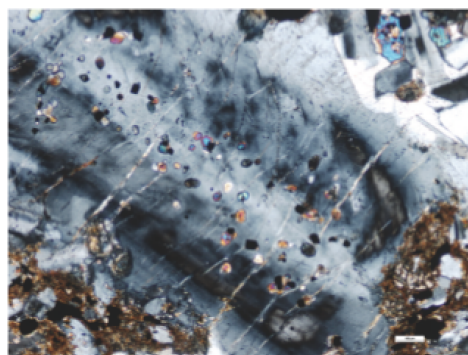
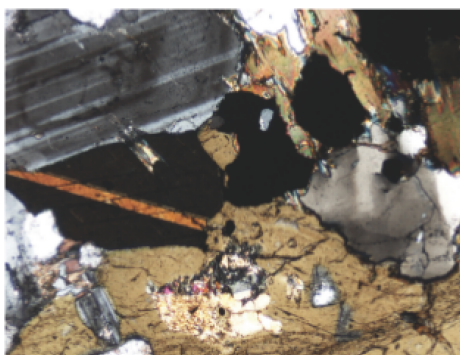


Figure 1



a

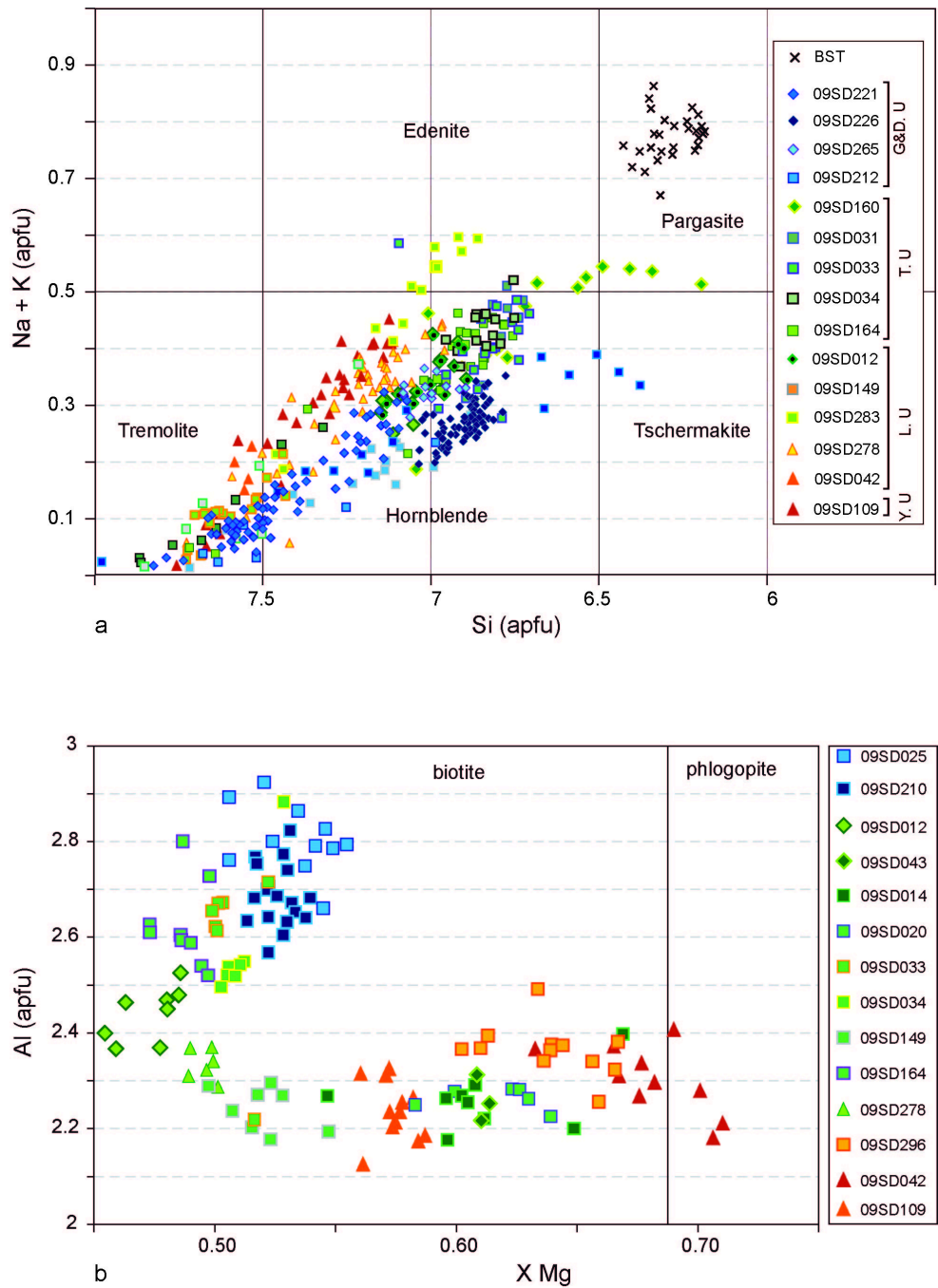


b

964

965 Figure 2





966

967 Figure 3

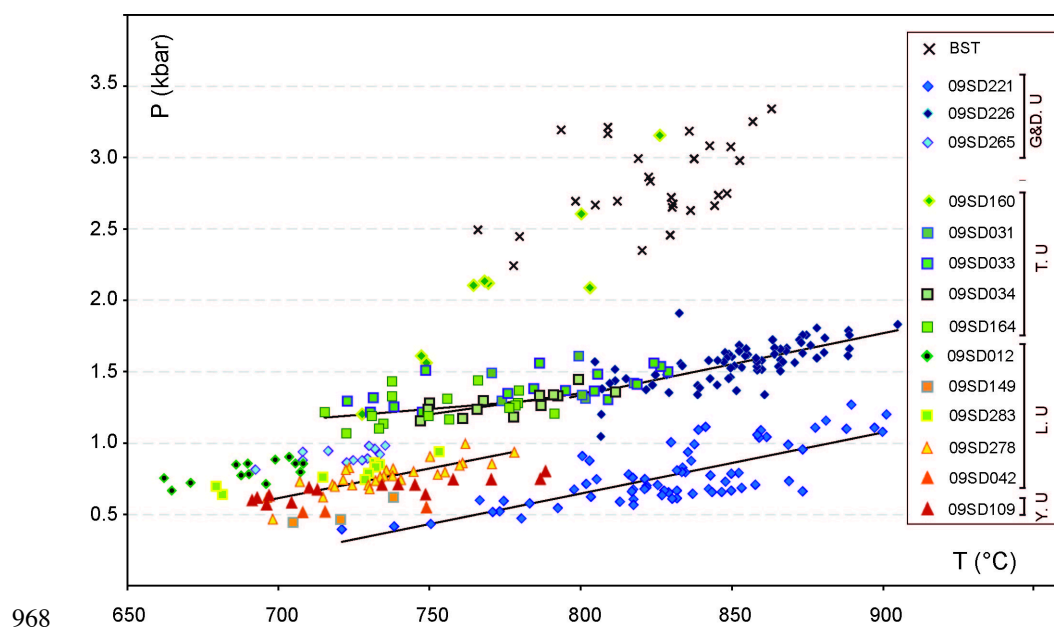
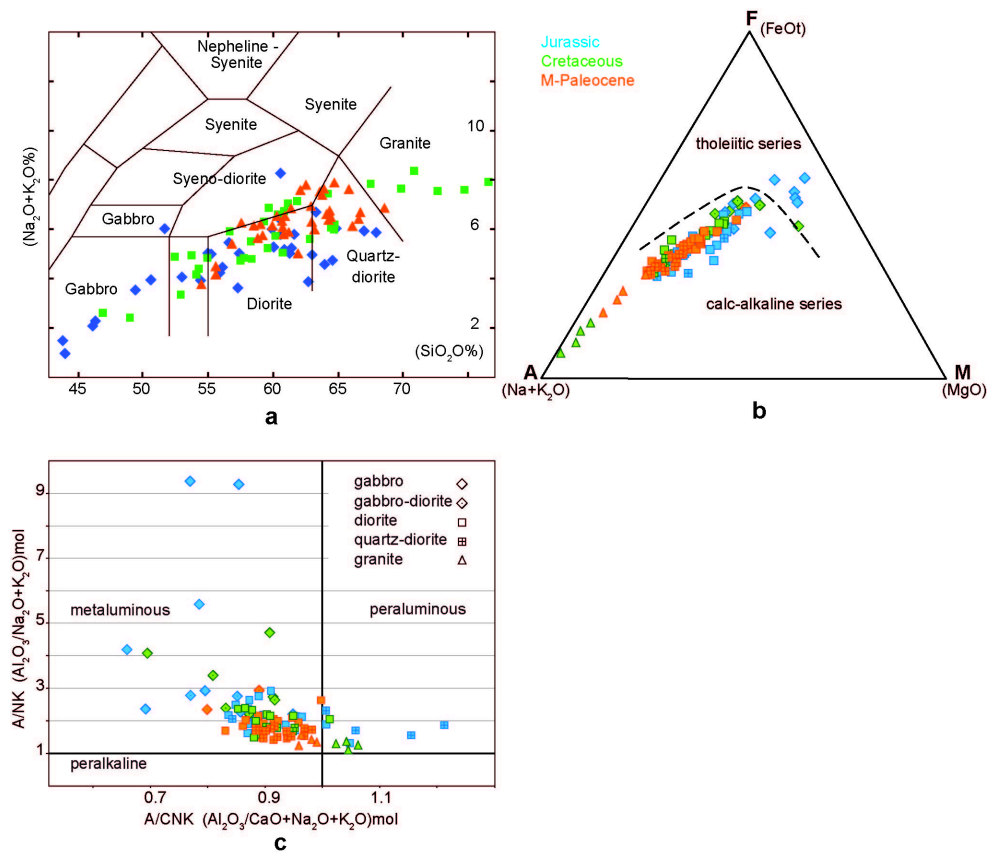


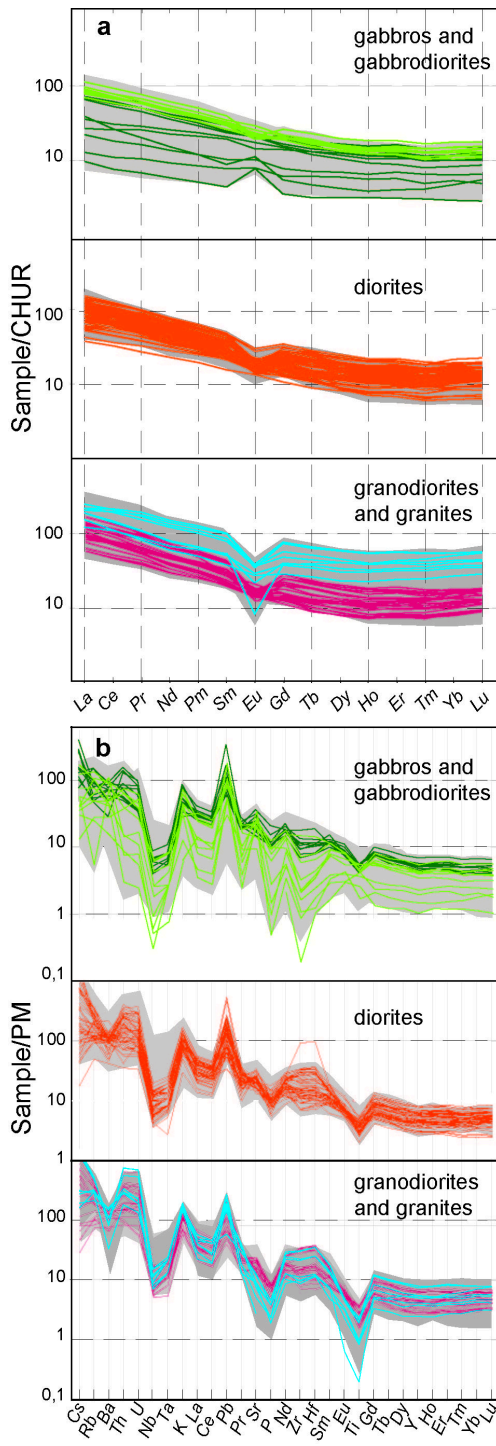
Figure 4





970

971 Figure 5

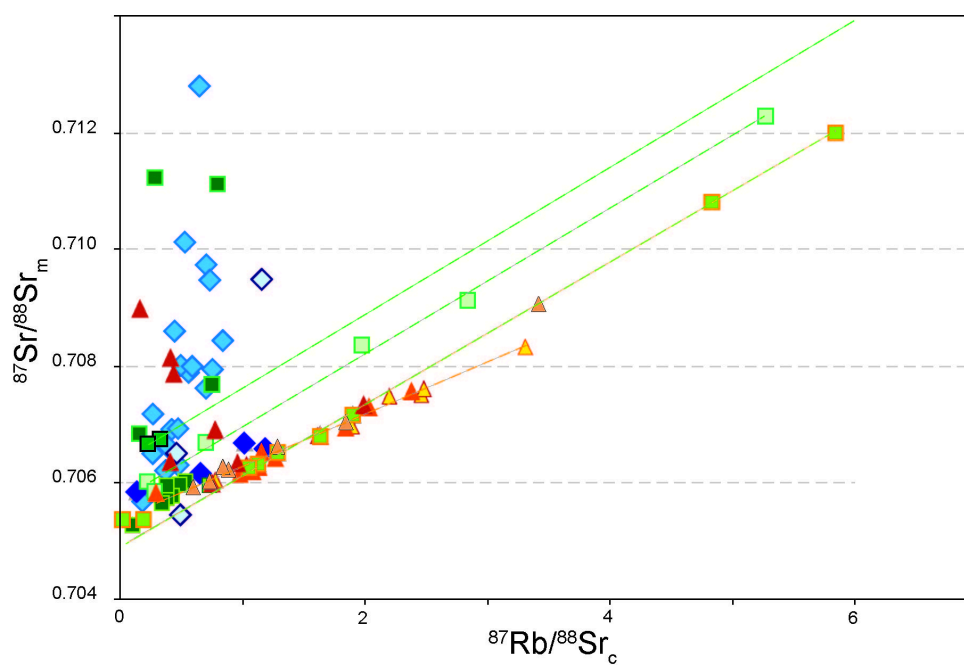


972

973 Figure 6



974



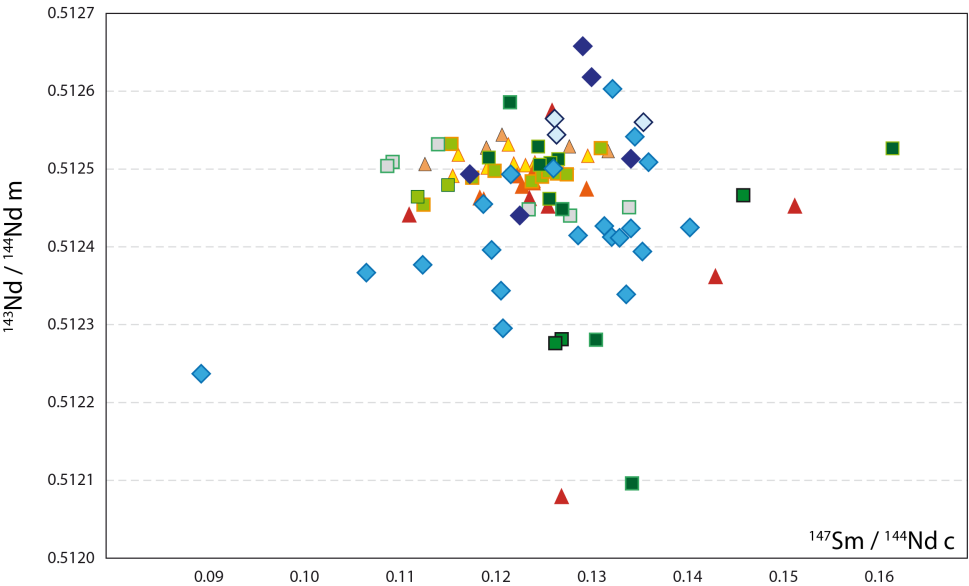
975

976

977 Figure 7

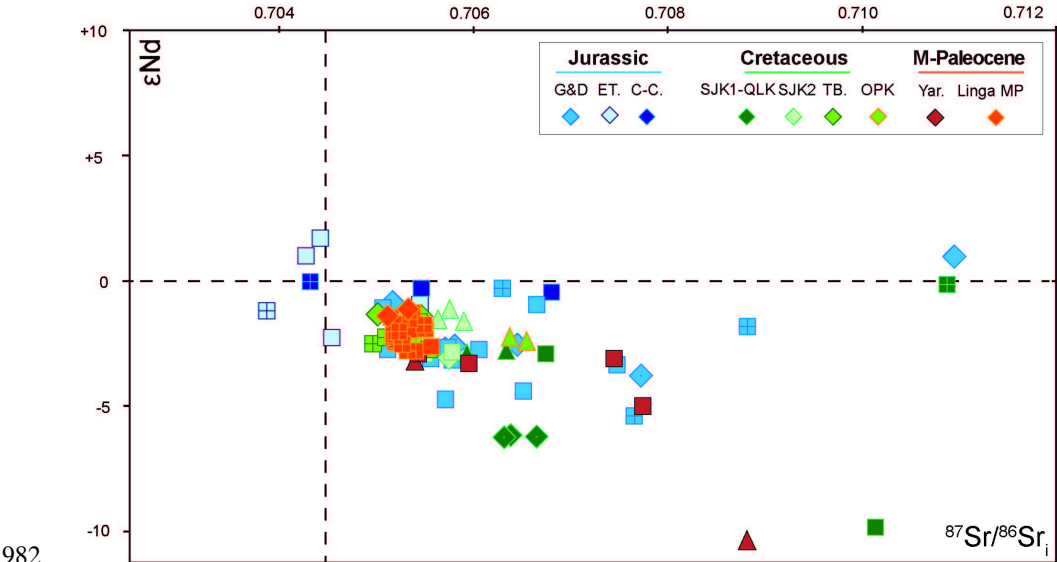
978

979



980

981 Figure 8



982

983 Figure 9

984

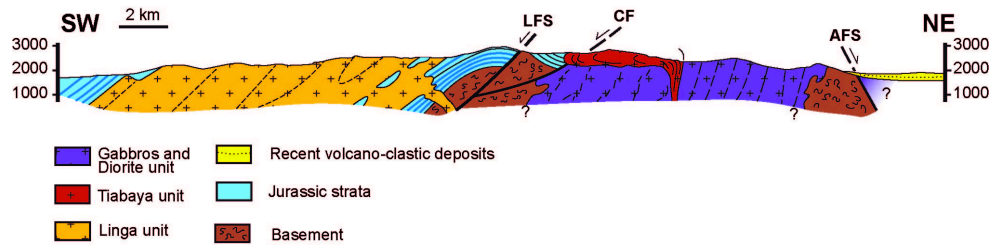


Figure 10

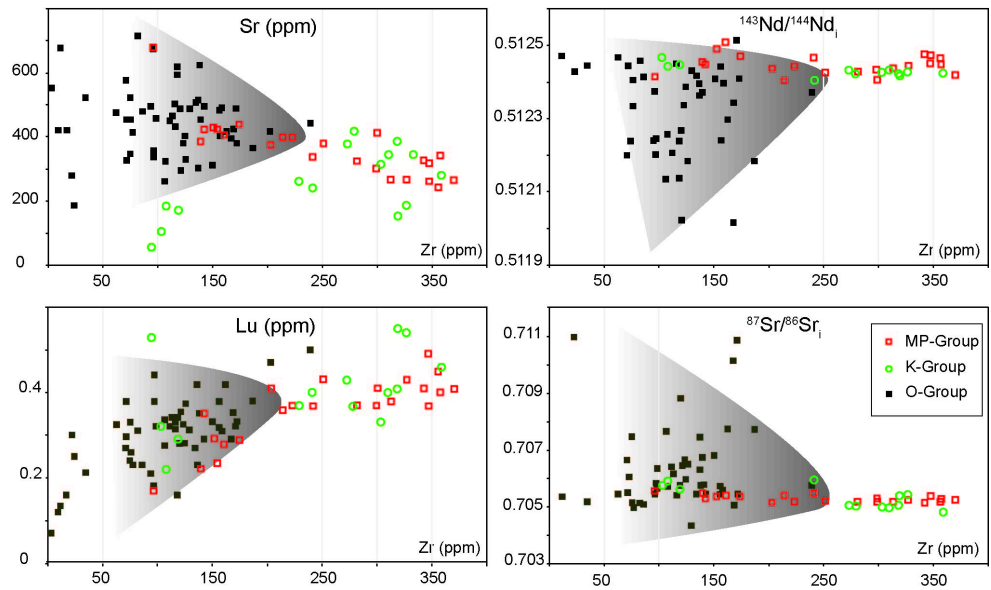


Figure 11



	Mineral phase	occurrence	composition
quartz and feldspar	quartz	interstitial grains and/or subhedral rounded crystal up to 2-3 mm in diameter	
	plagioclase	in every rock type with various habits, mainly as euhedral grains, either with grain size similar to the other minerals of the rock or as plurimillimeter-sized phenocrysts. Twins and zonations are ubiquitous. It generally exhibits normal zoning with sodic rims	An-content range is An <sub>92</sub> -An <sub>43</sub> for the gabbros and An <sub>53</sub> -An <sub>17</sub> for the granites
	alkali feldspar	in the felsic rocks - appears as anhedral, more or less perthitic grains in the groundmass as plurimillimeter-sized phenocrysts	Or <sub>99</sub> to Or <sub>79</sub>
Ferro-magnesian	pyroxene	in the mafic rocks (gabbro to diorite) and does not exceed 5 vol.% except for the gabbrodiorites of the Linga unit. It occurs both as isolated euhedral grains and more rarely as small rounded grains included into plagioclases (Figure 3a) in the mafic rocks (gabbro and gabbrodiorites). In the diorites, the pyroxene occurs as inclusion in the core of amphibole grains (Figure 3 b) The orthopyroxene is only present in the most mafic samples of the Linga unit (09SD12 and 09SD43) Clinopyroxene occurs in association with the orthopyroxene except in the more differentiated rocks devoid of orthopyroxene.	ranging from 52-61 mol % En, 36-45 mol % Fs and 2-3 mol % Wo compositions are quite homogeneous between Linga and Tiabaya (29-46 mol % En, 11-27 mol % Fs and 35-50 mol % Wo).
	amphibole	Green or brown amphibole is ubiquitous except for the Chapi-Churajón unit. It occurs as small to large-sized (up to 5 mm) euhedral grains, sometimes with inclusions of accessory minerals or plagioclase and twins features	amphiboles are calcic with CaO content >9.5 wt%. They are pargasite, tschermakite or magnesiohornblende in the mafic rocks, and edenite, hornblende or tremolite in the intermediate and felsic rocks (Figure 5).
	biotite	small to large (up to 5 mm) subhedral or euhedral crystals with various inclusions of accessory phases as Fe-Ti oxide, zircon and apatite. It constitutes up to 10-15 vol % of the mode of the different lithologies.	large range of XMg (0.45-0.71) for a limited Al <sub>2</sub> O <sub>3</sub> range (12-16 wt%)
accessory minerals	zircon	commonly found in the sample set and therefore was used for U-Pb dating. It occurs as prismatic bipyramidal, euhedral and highly transparent to slightly pink in color. The zircon sizes vary between 150 and 400 µm in length. Cathodoluminescence imaging shows that oscillatory zoning is prominent in the zircon population, and inherited cores occur in several samples.	
	fluorapatite	small prismatic crystals and are commonly found as inclusions in biotite and plagioclase, in gabbrodiorite to granitic facies.	41-43 wt% P <sub>2</sub> O <sub>5</sub> , 50-56 wt% CaO and 1.6-3.2 wt% F
	epidote	rare and small-sized isolated grains in the mafic to intermediate rocks.	
	titanite	not present in all of our sample set but occurs in all lithological types. It is abundant in some diorites and quartz-diorites (up to 2 vol% of the mode). It occurs mostly as isolated euhedral crystals, sometimes twinned and associated with hematite Fe-Ti oxides. Its chemical composition remains homogeneous between the facies	(TiO <sub>2</sub> range: 36.4-39.8 % ox.) but in the granites with slightly lower TiO <sub>2</sub> values (TiO <sub>2</sub> : 34.6-38.4 % ox.).
	oxydes	ubiquitous in all the rocks, and occur mainly as squared-euhedral crystal grains of magnetite and ilmenite, isolated or associated with ferro-magnesian phases. Hematite also occurs preferentially in the mafic rocks, and is sometimes affected by titanite veins. Ilmenite is found in association with hematite. Oxydes in general constitute less than 5 vol% of the mode of the rocks, mostly in the mafic lithologies, especially in the Gabbros and Diorites unit.	

995

996 Table 1